Anisotropic reticular chemistry

Wentao Xu[1], Binbin Tu[2], Qi Liu[3], Yufei Shu[3], Cong-Cong Liang[4], Christian S. Diercks[1], Omar M. Yaghi[1]✉, Yue-Biao Zhang[4]✉, Hexiang Deng[3]✉ and Qiaowei Li[2]✉

Abstract | Reticular chemistry has been focused on making simple structures in which a few kinds of components are linked to make crystals such as metal–organic frameworks (MOFs). While this chemistry has grown into a large field, a more extensive area with fascinating directions is emerging through the introduction of multiplicity and variation into the components of MOFs. When the MOF backbone is composed of more than two kinds of components, the resulting backbone multiplicity is regular repeats of those units. However, when variations involve multiple functionalization of the organic linkers or multiple metalation of metal-containing building units, it results in an aperiodic spatial arrangement of these variations, without altering the regularity of the MOF backbone. Such variance is represented by unique sequences of functionality or metal, and the very aperiodic nature of their spatial arrangement gives rise to anisotropy. These MOF constructs represent a new form of matter in which the sequences of such units are bound to an ordered backbone, thus adding complexity to an otherwise simple system, while preserving its overall crystallinity. It's worth noting that, when a molecule capable of either continuous or multistate anisotropic motion is integrated within a sequence in a MOF, the resulting property goes beyond what is possible in simple systems. We term this emerging area 'anisotropic reticular chemistry'.

[1]*Department of Chemistry, University of California, Berkeley and Kavli Energy NanoScience Institute, Berkeley, CA, USA.*

[2]*Department of Chemistry, Collaborative Innovation Center of Chemistry for Energy Materials (iChEM) and Shanghai Key Laboratory of Molecular Catalysis and Innovative Materials, Fudan University, Shanghai, China.*

[3]*Key Laboratory of Biomedical Polymers, Ministry of Education, College of Chemistry and Molecular Sciences, The Institute of Technological Sciences and The Institute for Advanced Studies, Wuhan University, Wuhan, China.*

[4]*School of Physical Science and Technology, ShanghaiTech University, Shanghai, China.*

✉*e-mail: yaghi@berkeley.edu; zhangyb@shanghaitech.edu.cn; hdeng@whu.edu.cn; qwli@fudan.edu.cn*

https://doi.org/10.1038/s41578-020-0225-x

Synthetic crystals are considered simple, in that they are repeating patterns of few constituents throughout. Although crystalline materials are useful in many endeavours, the need exists for making chemical structures that can perform more sophisticated operations. This level of sophistication may require structural features largely absent in synthetic materials, such as spatially arranged compartments that are open to each other, yet function differently and across different timescales, capable of counting and sorting chemical information, and operating sequentially or in parallel. In considering natural systems and how they carry out such complex operations, one finds that their multicomponent constitution is paramount. The challenge in synthetic systems is that the introduction of multiple components into crystals, whether extended or molecular, results in phase separation, while in amorphous systems, such as polymers, modifying their backbone or side chains leads to reorganization of their structures. In other words, multicomponent synthesis suffers from either phase separation or lack of structural control.

The advent of reticular chemistry[1,2], the linking of molecular building blocks by strong bonds to make crystalline extended structures, has changed this state of affairs in a profound way, principally because well-defined building units are used. This chemistry is best illustrated in the case of metal–organic frameworks (MOFs), in which secondary building units (SBUs)[3] are linked by organics into crystalline two-dimensional[4] and three-dimensional[5] frameworks. The fact that the organic linkers have multiple metal-binding linkages results in multi-metallic, rigid and directional SBUs, aspects that impart a high level of control over the resulting structures. Additionally, because the linkages are an integral part of the SBU, they provide for MOFs with different SBU metal composition and geometry.

The thermodynamic minimum driven by the strong linkages and the directionality of the SBU allows for the design of a specific structure, while limiting the number of possible structural outcomes and avoiding amorphous mixtures. In the case of de novo synthesis of MOFs with multiple linkers, the tendency is for all the different linkers to be incorporated within one structure to make a multicomponent MOF. This outcome is easily understood, especially when the linkers are based on one kind of linkage (for example, carboxylate) with similar pK_a values, and when such linkers are not subject to other limitations, such as steric hindrance (for example, linker–linker interactions), as is the case in zeolitic imidazolate frameworks (ZIFs)[6,7]. On this basis, the problem of phase separation is overcome in the synthesis of multicomponent MOFs. Considering the variety of possible compositions and geometries of SBUs in MOFs, together with the possibility of functionalizing

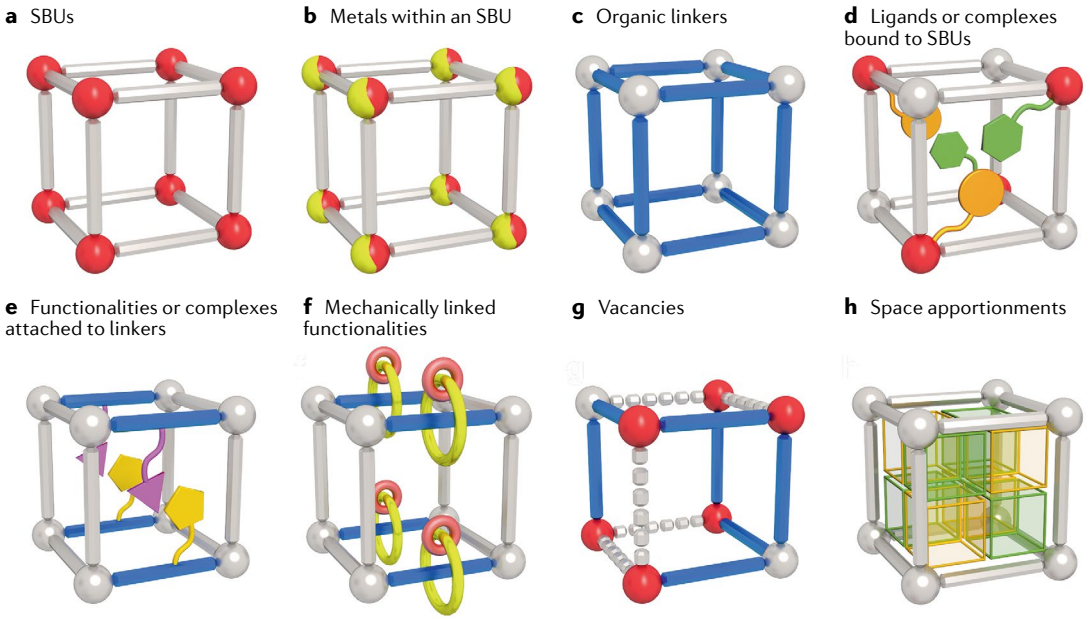

Fig. 1 | **Molecular components in metal–organic frameworks (MOFs). a** | Polynuclear clusters (red spheres) are defined as secondary building units (SBUs) and form the nodes of the framework. **b** | Metal sites in an SBU could be occupied by multiple kinds of metal ions, illustrated in yellow and red. **c** | Linkers (blue rods) are organic molecules that connect SBUs together to form reticular structures. **d** | Terminal ligands or complexes (in green and orange) bound to the metals in SBUs are a form of components attached to the backbone of the framework. **e** | Organic functionalities or coordination complexes (in purple and yellow) attached to the linkers are another form of components attached to the MOF backbone. **f** | When mechanically linked functionalities are employed as components for MOF construction, motion and dynamics in MOFs are expected. **g** | Vacancies are introduced when organic linkers and/or inorganic SBUs are missing from their expected positions (dashed cylinders and grey spheres), representing a special kind of MOF component. **h** | When extraneous components are installed into the parent framework and divide the pores, space apportionments (shown as green and orange cubes) are achieved.

the organic linkers, MOF crystals can no longer be thought of as simple. In concept, the variance that can be created in the backbone of MOFs is likened to that of the amino acids in proteins, and when the variance pertains to the covalent functionalization of the MOF backbone, it resembles the nucleotides in DNA. In both of these scenarios, the variance colludes to create sequences of information that code for specific operations.

In a way, the ability of variance to create unique sequences of chemical information along a certain direction, which also enables directional operations, let's say in a MOF crystal, is a form of anisotropy — a property imposed by variance and realized along a specific direction. While MOFs are not yet as sophisticated in their operations as proteins and DNA, the chemical basis for transferring these concepts into their structure is not outside the realm of possibility. Evidence that such anisotropy in crystals is real and articulating the foundation of its emergence is the subject of this article.

Specifically, we outline strategies for making multicomponent MOFs and creating variance in both organics and metal-containing units. We show how the variance in composition and structure thus created is an essential part of what we term anisotropic reticular chemistry and define as reticular chemistry of structures having anisotropy in constitution giving rise to operations along a specific direction. It is worth noting that, even though, up to this point, most MOFs have been composed of very limited kinds of components, they have already shown outstanding physical and chemical properties[8–39]. Anisotropic reticular chemistry is already pointing to a new level of control and sophistication in MOF structures and operations.

Variance leading to directionality

The elements of anisotropic reticular chemistry originate from multicomponent structures, where, in the case of MOFs, the components are defined on the molecular level (FIG. 1). They are SBUs, metals within an SBU, organic linkers, organic ligands or metal complexes bound to SBUs, and organic functionalities or metal complexes, including mechanically linked functionalities, attached to organic linkers. We also consider as components vacancies and space apportionments created in MOFs. Although weakly bound guest molecules or counter ions are components, they are not the focus of this contribution. While MOF-based structures at the macroscopic scale, such as core–shell structures and MOF–polymer composites, are fascinating, their components are not molecularly defined in the same way as MOF crystals covered in this Review. The reader is referred to literature reviews[40,41] on MOF-based architectures and hybrid materials.

It is instructive to group these components as being part of the backbone or functionality, each of which has its own set of variances. The backbone is the 'stripped-down' version of the fundamental building units in the MOF that are linked and, therefore,

essential for its structural integrity. The backbone does not include functionalities attached to the MOF or metal ions that might be bound to an organic linker, such as in a porphyrin. Generally, backbone variance is created by: having the alternation of SBUs and linkers follow different patterns along different directions; linker or metal vacancies whose spatial arrangement is either ordered or disordered; and installing extraneous components into a parent backbone with all else unchanged (FIG. 2).

Now, we turn to the variance in functionalities and in metals (FIG. 2). Such variances are created by either mixing more than one functionality or more than one metal either de novo or by post-synthetic modification in one MOF. The termed functionality variance and metal variance include the mixed organic functionalities, mixed metals in an SBU and metalation of organic linkers or SBUs. Functionality variance and metal variance are usually crystallographically disordered, although, as will be discussed, ordered arrangements of mixed linkers or mixed metals are observed in a few cases.

When the variance in either the backbone or the functionality is disordered, it is most likely to be a unique sequence of spatially arranged chemical entities (metals or organic functionalities). These sequences are necessarily directional, just as nucleotides in DNA. This anisotropy is further elaborated below with specific examples, including how it forms the basis for unusual gas storage and separation properties, enzyme-like selective catalysis and introduction of directional dynamics within MOFs.

Backbone variance and directionality

This section describes MOFs in which backbone variance is observed by having more than one kind of SBU and linker in the backbone (namely, multinary MOFs). It also includes variance introduced by linker and SBU vacancies in the backbone and linker installation into a MOF. The spatial arrangement of components along a specific direction dictated by variance is also discussed.

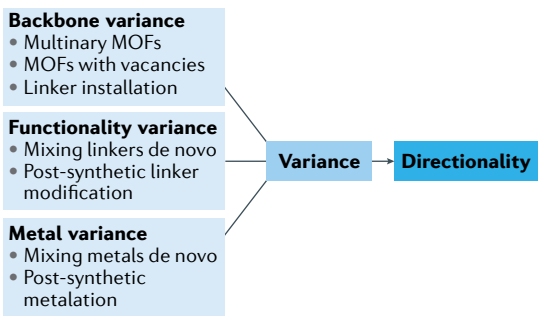

Fig. 2 | **Emergence of anisotropic reticular chemistry.** In reticular chemistry, structural variance can be realized in three categories: backbone variance (more than one kind of secondary building unit and linker in the metal–organic framework (MOF) backbone), functionality variance (mixed organic functionalities attached to the backbone) and metal variance (mixed metals in secondary building units or mixed metalation of linkers). These variances lead to unique sequences of spatially arranged chemical entities along specific directions, and reticular structures with directionality give rise to operations in anisotropy.

Multinary MOFs

A MOF constructed from one kind of SBU and one kind of organic linker gives a binary structure. To date, most MOFs reported can be classified as members of this category. Multinary MOFs are constructed from more than two such building units. Variance can be imparted by the presence of multiple linkers (that is, alteration in geometry or metrics) and/or the presence of more than one kind of SBU (that is, variation in metal composition or geometry)[40,42–46]. In this context, the term multinary is used to emphasize that the distinct inorganic and organic building blocks precisely meet the geometric and metric requirements to be embedded in a periodic net at topologically distinct sites as nodes and edges, thus achieving long-range order. Pillared-layer MOF structures[47–49] incorporate variance within and between the layers. Typically, within the layers, there are carboxylate linkers and, between the layers, there are weakly bonded bipyridine-type linkers. The bond energy of metal–carboxylate (150–400 kJ mol^{-1}) is significantly higher than metal–pyridine (40–200 kJ mol^{-1})[1]. In this Review, we are concerned with systems in which the backbone is entirely composed of strong bonds. The concept of strong bonds is evidenced by the extremely large number of metal–carboxylate MOFs reported, and is further extended to other charged linkers, such as pyrazolates and imidazolates. The architectural robustness achieved by the strong bonds has a tremendous impact on the favourable properties of MOFs.

Multinary MOFs with multiple linkers. The first multinary MOFs were made by constructing frameworks from more than one type of organic linker. UMCM-1 (**muo**)[50], UMCM-2 (**umt**)[51], UMCM-3 (**koh**)[52] and MOF-205 (DUT-6, **ith-d**)[53,54] are ternary MOFs constructed by stitching 6-connected $Zn_4O(COO)_6$ SBUs with trigonal tritopic 1,3,5-tris(4-carboxyphenyl) benzene (BTB), as well as with additional ditopic linkers of various length (1,4-benzenedicarboxylate (BDC), thieno[3,2-b]thiophene-2,5-dicarboxylate (T^2DC), 2,5-thiophenedicarboxylate (TDC) and 2,6-naphthalenedicarboxylate (NDC)), respectively (FIG. 3a). As a consequence of their ternary composition, the frameworks feature multiple kinds of mesopores and micropores. MOF-210 (**toz**)[53] and DUT-60 (**ith-d**)[55] have heterodual nets, and, therefore, are not prone to framework interpenetration (FIG. 3a). Ternary DUT-60 features the highest accessible pore volume (5.02 $cm^3 g^{-1}$) and gravimetric surface area (7,800 $m^2 g^{-1}$) of any MOF.

Multinary MOFs are not limited to ternary structures. The first quaternary MOF, termed MUF-7a, was constructed by coordinating 6-connected $Zn_4O(COO)_6$ SBUs with tritopic BTB linkers and two metrically distinct ditopic linkers, BDC and 4,4′-biphenyldicarboxylate (BPDC), to form a framework with an underlying **ith-d** net[56] (FIG. 3b). The three kinds of linkers in MUF-7a allow one linker to be modified but not the other, and, in turn, the corresponding pores were functionalized without altering other pores. Accordingly, the framework was functionalized to have catalytic pockets where one organic linker with prolinyl group serves as the

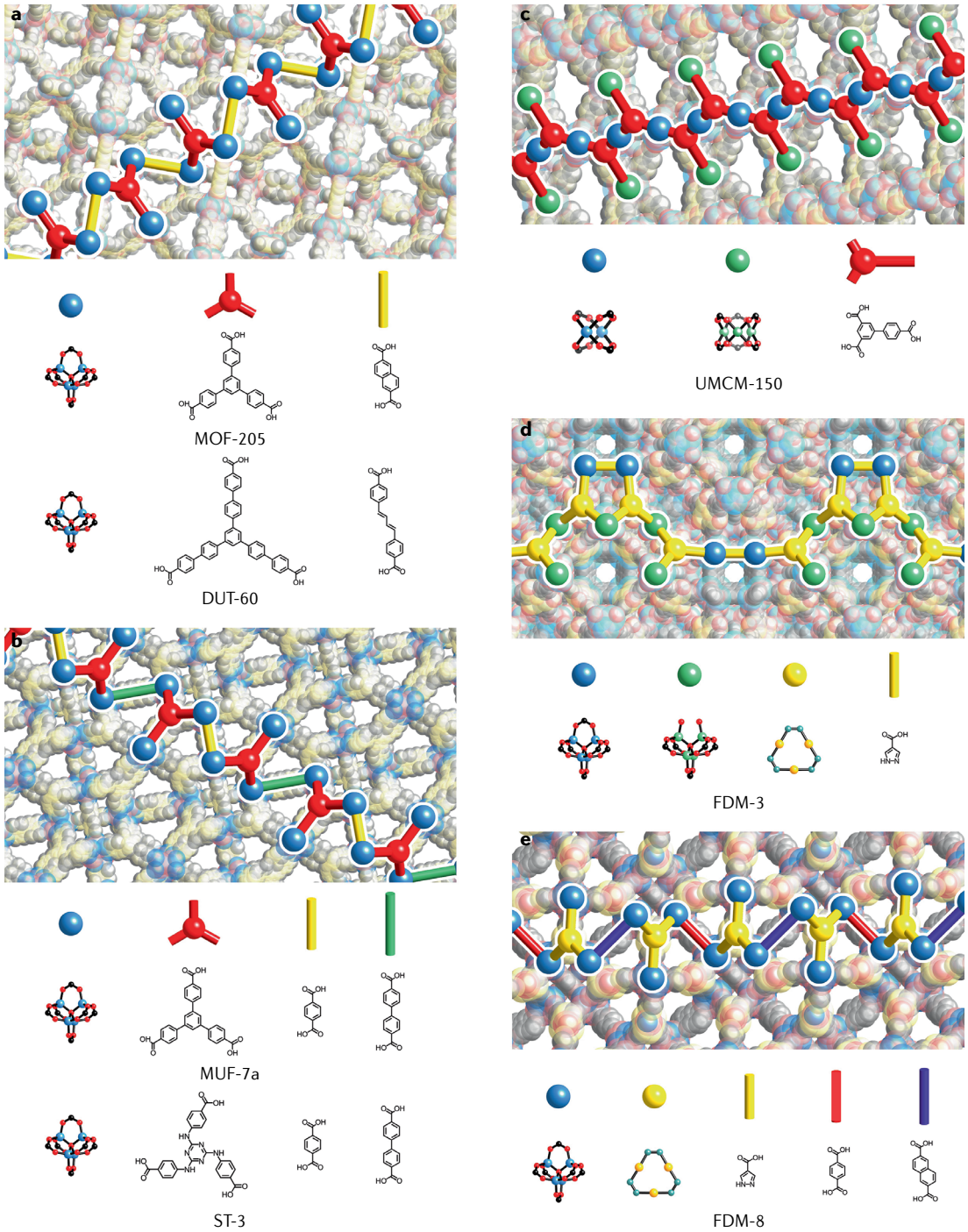

Fig. 3 | **Backbone variance in multinary metal–organic frameworks. a** | MOF-205 (aka DUT-6)[53,54] and DUT-60 (REF.[55]) are constructed by one kind of secondary building unit (SBU) and two kinds of organic linkers with different geometry. **b** | MUF-7a (REF.[57]) and ST-3 (REF.[58]) feature one kind of SBU and three different types of organic linkers with different metric and geometric parameters. **c** | UMCM-150 (REF.[59]) has one square planar SBU, one trigonal prismatic SBU and one organic linker. **d** | FDM-3 (REF.[61]) is composed of three different types of SBUs and one organic linker. **e** | Backbone variance in quinary FDM-8 (REF.[64]) is dictated by two kinds of SBU and three kinds of organic linkers. Ternary MOF-205, quaternary MUF-7a and quinary FDM-8 share the same net topology, but the complexity of backbone variance increases along with the incorporation of more components into the net.

catalytic site and the other two linkers define the pore environments[57].

The challenge in constructing multinary MOF is that the building units, if chosen to be rigid, must have the exact metrics and geometry to fit together to form the target structure. However, if they are flexible, the likelihood of making a multinary MOF is dramatically enhanced. Using the flexible tritopic linker 4,4′,4′′-*s*-triazine-1,3,5-triyltri-*p*-aminobenzate (TATAB) with one or two kinds of ditopic linkers (BDC,

NDC or BPDC) results in ternary ST-1, ternary ST-2 and quaternary ST-3 MOFs[58] (FIG. 3b). In addition, this flexible linker strategy has led to the quaternary framework ST-4 of **ott** topology. These frameworks show promise in high-pressure methane storage, with ST-2 having the highest methane deliverable capacity (289 $cm^3_{STP}\,cm^{-3}$ (567 $mg\,g^{-1}$) at 298 K and 5–200 bar), surpassing previous records.

Multinary MOFs with multiple SBUs. Linking more than one kind of SBU can also make multinary MOFs. UMCM-150 (REF.[59]) is a ternary MOF constructed from triangular biphenyl-3,4′,5-tricarboxylate (BHTC), which is linked into the (3,4,6)-connected **agw** net from two geometrically distinct SBUs: 4-connected square planar $Cu_2(COO)_4$ and 6-connected trigonal prismatic $Cu_3(COO)_6$ SBUs (FIG. 3c). This framework was achieved by employing isophthalates and benzoates as coordinating moieties. Similarly, the design of multinary MOFs with SBU alteration is obtained by using heterotopic linkers providing different coordinating linkages, such as linkers having both azolates and carboxylates. **rht**-MOF-1 (REF.[60]) is a ternary MOF constructed from 5-tetrazolylisophthalate (TZI), 4-connected square planar $Cu(COO)_4$ and 3-connected triangular $Cu_3(\mu_3\text{-}O)(NN)_3$ SBUs to form a framework with underlying (3,3,4)-connected **ntt** net.

An example of MOFs with multiple SBUs of two different metals is FDM-3 with (3,5,6)-connected **ott** net[61], which is a quaternary MOF constructed from 4′-pyrazolecarboxylate (PyC) and three kinds of geometrically distinct SBUs (triangular, square pyramidal and octahedral). Specifically, the triangular SBUs are based on Cu(II), while both the square pyramidal and the octahedral SBUs are based on Zn(II) (FIG. 3d).

Combining both multiple linkers and multiple SBUs in one MOF structure represents a synthetic challenge, because the possibility of multiple phases is dramatically increased with increasing number of components. Recently, two quaternary MOFs[62] (FDM-6, **umt** net and FDM-7, **ith-d** net) were obtained by linking $Zn_4O(COO)_6$ and $Cu_3(NN)_3$ SBUs with ditopic PyC and BDC (or NDC) linkers. These multinary MOFs display both linker and SBU variance in the backbone and, thus, elevate multinary frameworks to the next level of complexity. This strategy is also implemented in making MOF-818 and MOF-919 (REF.[63]), in which trigonal prismatic $Zr_6(\mu_3\text{-}O)_4(\mu_3\text{-}OH)_4(COO)_6$ or $M_3(\mu_3\text{-}O)(COO)_6$ (M = Fe, Sc, Al) and triangular $Cu_3(\mu_3\text{-}O)(NN)_3$ are linked by PyC to yield ternary frameworks with underlying (3,6)-connected **spn** or **moo** net. MOF-818 shows excellent chemical stability across a broad pH range and features a supertetrahedral mesoporous cage with 18 vertices, allowing for accommodation of large biomolecules such as vitamin B_{12} or insulin. It is clear from the foregoing discussion that large pores can be produced from short linkers when multinary MOFs are targeted, obviating the need for longer linkers.

Multinary MOFs with the most kinds of components reported to date are FDM-8 and its derivatives[64]. In FDM-8, five different components, two inorganic SBUs with different geometries (octahedral $Zn_4O(COO)_6$ and triangular $Cu_3(NN)_3$) and three organic linkers with distinct length and coordinating functionality (PyC, BDC and NDC), are linked into a crystal, with each constituent sitting at crystallographically well-defined positions (FIG. 3e). This study demonstrated the increasing sophistication with which different chemical functionality can be placed along a specific direction and how it enables the frameworks to guide guest species along well-defined pathways within the crystal.

MOFs with vacancies

Vacancies in MOFs, where organic linkers and/or inorganic SBUs of the backbone are missing from their expected positions, constitute a special case of anisotropy in frameworks. The building units of MOFs generally have a high connectivity, thus endowing them with high tolerance for vacancies, without resulting in structural collapse. Vacancies can be introduced by design and the impact of their variation with respect to size, concentration, chemical environment and spatial distribution represents an important aspect of anisotropic reticular chemistry.

Backbone vacancies resulting from modulators. UiO-66 is a prototypical example of frameworks that have vacancies in their backbone. Terminal modulators such as CH_3COOH or HCOOH (REF.[65]), which are added to the reactant to improve crystallinity, compete with organic linkers for coordination sites, and, thus, create sites capped by the modulators[66,67]. These sites can be viewed as linker vacancies in the resulting frameworks. A significant amount (up to ~10%) of linker vacancies are created using this modulator approach. Similarly, mixing pristine organic linkers with a second linker of lower topicity is found to create linker and/or inorganic SBU vacancies in MOFs while retaining the essential topology of the parent framework[68]. In a more systematic approach, tetratopic linkers are partially replaced by pairs of tritopic and monotopic linkers, and the vacant sites in between the pairs provide varied and tailored pockets for incoming metal ions[69]. In addition, partially interpenetrated frameworks also demonstrate the concept of vacancies[70]. It is worthy of note that anisotropic arrangement of mesopores[71] and encapsulating nanoparticles in MOFs by templating and surface techniques[72] were achieved. While the vacancies derived from such structures are not precisely defined, methods used to superimpose anisotropic arrangement can potentially be applied later to introduce directionality to the MOF system at a molecularly defined level.

It was initially presumed that the linker and inorganic SBU vacancies were distributed randomly in the UiO-66 series. However, nanodomains with correlated inorganic SBU and linker vacancies in UiO-66(Hf) were later discovered[73]. Specifically, nanodomains of missing inorganic SBU in UiO-66 were found to have **reo** net or **scu** net[74] (see the section on ‘Mapping the spatial arrangements’). The exact formation mechanism of these vacancies remains unknown, but it was observed that such vacancies evolve with crystallization time, demonstrating interesting non-equilibrium transformations in these solids.

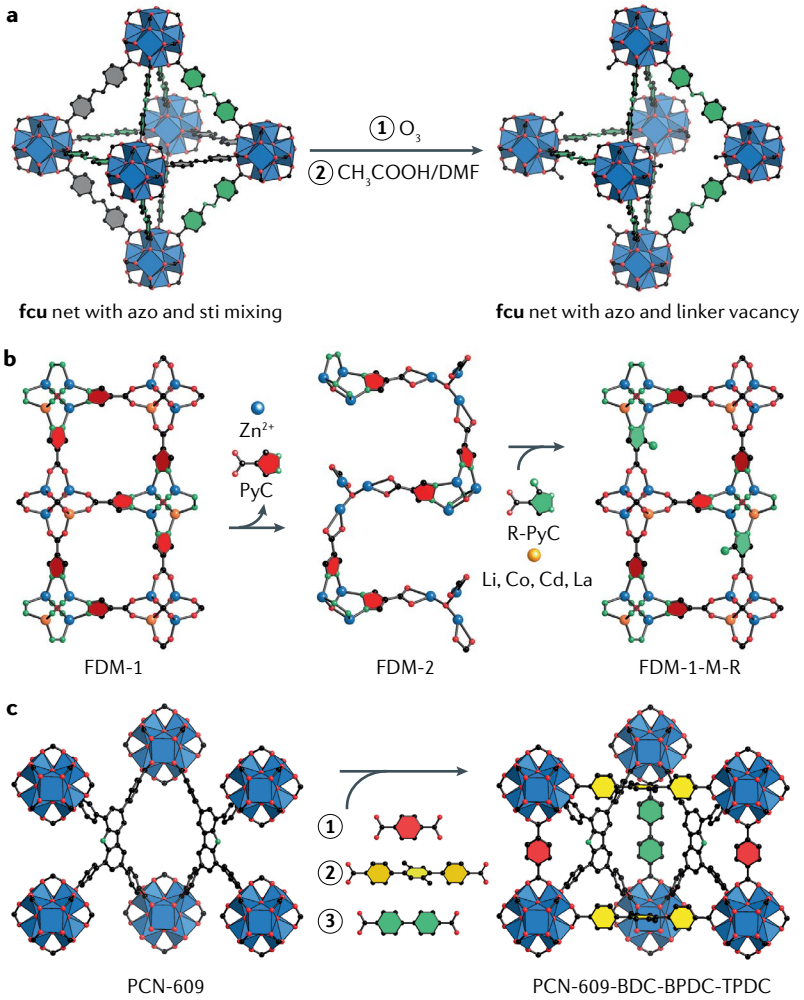

Fig. 4 | **Structure editing for backbone variance in metal–organic frameworks. a** | In a Zr-based metal–organic framework with mixed linkers (4,4′-azobenzene dicarboxylate (azo) and 4,4′-stilbene dicarboxylate (sti)), azo linkers with cleavable olefin bonds are removed by ozonolysis, followed by solvent washing, and linker vacancy is created in the backbone[81]. **b** | Ordered vacancies are generated in FDM-1 by removing half of the organic linkers and a quarter of the metal ions. The vacancies could be further filled by new metal ions and new organic linkers[82]. **c** | By sequential linker installation on PCN-609, the structure editing results in four different kinds of organic linkers arranged anisotropically in a single crystal[85].

Structure editing. In addition to the formation of vacancies during solvothermal synthesis of MOFs, post-synthetic structure editing of MOFs provides an alternative approach to the generation of vacancy sites in the backbone. Exposing MOFs to acid etching or hydrolysis can create vacancies by breaking the linkage between metal ions and organic linkers, and, using this approach, mesopores and macropores are generated[75,76]. However, these strategies generally lack control with regard to the concentration and size of vacancies, and their arrangement in the crystal.

Mixing two kinds of organic linkers de novo in a MOF single crystal, followed by selective removal of one type of linker, can produce vacancy components in the parent MOF without affecting the integrity of the framework[77–79]. Here, the size, concentration and distribution of the vacancies are predetermined by both the position and the number of labile linkers in the mixed-linker MOF. Two prominent examples include the splitting of imine-based linkers by hydrolysis[80] and the ozonolysis of linkers containing cleavable olefin bonds[81] (FIG. 4a). In both systems, the labile linkers were mixed with inert linkers to synthesize mixed-linker MOFs. Upon hydrolysis or ozonolysis, the labile linkers were cleaved and the linker fragments subsequently removed by washing or sublimation. Such selective structure editing on the backbones triggers the fusion of micropores into mesopores and improves gas sorption and catalytic properties through the fine-tuning of vacancy concentrations in the frameworks.

In addition to linker discrimination based on chemical stability, an example of site-selective component removal in a simple MOF with only one metal and one linker has been reported[82]. Here, half of the organic linkers (PyC) and a quarter of the metal ions (Zn^{2+}) were removed in an ordered manner from the parent FDM-1 framework with an underlying **pcu** net, affording an entirely new structure of **srs** topology, termed FDM-2 (FIG. 4b). One intriguing point of this study is that all linkers were initially crystallographically equivalent, and only half of these linkers were removed upon structure editing in a highly ordered way. The resulting net is a lacunary version of the original net, analogous to niobium oxide (NbO), which can be described as a rock-salt structure with ordered vacancies.

Linker installation

In many MOFs, capping modulator molecules or terminal ligands (for example, OH^- and H_2O) occupy well-defined coordination sites of the SBUs. As a result, these frameworks feature SBUs with lower connectivity. Such sites can be considered as ordered linker vacancies of the idealized, maximally connected framework. When the size and orientation of the vacancy match those of an extraneous organic linker, it can be installed post-synthetically on the vacancy site. During this linker installation, the original cell metrics remain essentially unaltered. Designing multiple kinds of vacancies in one MOF allows multiple linker installations to be performed in sequence, thus providing an alternative method to construct multinary MOFs.

Based on FDM-2 with ordered vacancies[82] (FIG. 4b), new linkers such as 3-methylpyrazole-4-carboxylate (CH_3-PyC) could be installed into the vacancy sites, and a multinary MOF isoreticular with FDM-1 but with two kinds of organic linkers arranged in an ordered manner is achieved. PCN-700 (REF.[83]) with **bcu** net has the 8-connected $Zr_6O_4(OH)_8(H_2O)_4$ SBUs as the nodes. By replacing terminal OH^- and H_2O ligands attached to the SBUs with extraneous ditopic carboxylate linkers, connecting numbers of the SBUs increase to 10 or 12. As a result, new linkers with new functionalities can be pinpointed in the single crystal with precision. The size-matching between the linkers and the vacancy sites is proved to be crucial for successful linker installation.

Employing sequential linker installation with up to three different kinds of extraneous linkers of different length has been demonstrated in the two **scu** topology frameworks NPF-300 (REF.[84]) and PCN-609 (REF.[85]) (FIG. 4c). Stepwise substitution of terminal ligands on the

8-connected Zr-based SBUs with three kinds of ditopic linkers yielded new frameworks with 12-connected SBUs. In both cases, the length of the extraneous linkers was adjusted carefully to allow for bridging of specific crystallographically defined SBUs around vacancy sites. As a consequence, the installation process is rendered directional, which enables anisotropic incorporation of different linkers along specific directions within the crystal lattice.

Post-synthetic installation of extraneous linkers has been exploited for molecular retrofitting of MOFs to increase their mechanical stability. MOF-520 (REF.[86]) is composed of 8-connected Al-based SBUs linked by tritopic BTB linkers. In each octametallic SBU, the octahedral Al in the circular cluster share corners through eight OH^- and four $HCOO^-$ ligands. The distance and relative orientation between the $HCOO^-$ ligands from two neighbouring SBUs provide ideal sites for BPDC linker installation. The new MOF after retrofitting could maintain crystallinity under hydrostatic pressure up to 5.5 GPa.

It was demonstrated that the extraneous linkers to be installed into the parent framework can be templated by the framework itself. Specifically, pyridyl ligands bearing unsaturated functional groups (cyano, ethynyl and vinyl)[87] were found to undergo cyclotrimerization reactions when anchored to the coordinatedly unsaturated metal sites of the $Fe_3(\mu_3\text{-}O)(COO)_6$ SBUs in the MOF, resulting in pore apportionment by the in situ formed tripyridyl linkers. These cyclotrimerization reactions require elevated temperatures and transition-metal catalysts when carried out in solution, but occur under mild conditions with no catalyst in the MOF pores. The observation can be attributed to steric clashing of three substituents owing to geometric constraints, reminiscent of the catalytic transformation of substrates within enzyme pockets.

Functionality variance and sequences

In backbone variance, the structural anisotropy is imparted by alteration in the backbone, through multinary MOFs, vacancies and linker installation. Beyond variance in the MOF backbone, multiple types of functional groups (functionality variance) and metal components (metal variance) can be introduced into the same crystal without altering the underlying backbone structure[88]. MOFs of this class were generally termed 'multivariate MOFs' (MTV-MOFs). In MTV-MOFs with functionality variance and metal variance, the anisotropy originates from different functional groups appended to the backbones but without changing the framework topology, and the variation of SBUs without altering their linkage across the backbone, respectively.

It is worth noting that MTV-MOFs must not be mistaken for solid solutions, where one component, a solute, is closely surrounded by and exchangeable with the major component, a solvent. The strong bonds across the entire MOF backbone fix the organic linkers at specific crystallographic positions and separate them from each other. Although interaction may exist between adjacent organic linkers through the functional groups they carry, the strong bond between the linker and the SBU makes the positional exchange of entire linkers unlikely to take place within the crystal structure in solvent-free form. As such, MTV-MOFs bear closer resemblance to the sequence of amino acids in proteins and the bases in DNA, neither of which would be described as a solid solution.

The fixed position of functionalities and metals in MTV-MOF provides the foundation for the possible sequence generated by their spatial arrangement of functionalities and metals along a specific direction. However, it does not rule out the possibility of random distribution. As a matter of fact, the arrangement of functional groups was rarely discussed or was mainly considered to be random in the early works of MOFs synthesized by mixing linkers of the same size and linkage[89–92]. The possibility of spatial arrangement of functionalities was suggested by the discrepancy between the input linker ratio for the synthesis and the resulting ratio in MTV-MOF-5 (REF.[88]). The nonlinear correlation between the gas-adsorption property and linker ratio in MTV-MOFs strongly pointed out the existence of spatial-arrangement functional groups along a specific direction, plane or three-dimensional space across the MTV-MOF crystal, hence, the formation of a unique sequence[88,93,94].

In this section, different forms of functionality variance and synthetic strategies are discussed, while metal variance is discussed later. For a given combination of functional groups as the functionality variance for MTV-MOFs, both the ratios between them and their spatial arrangement at specific directions across the crystal led to additional anisotropy of MOFs[44,94,95]. There are two general strategies to introduce functionality variance in MOFs, both of which involve the use of differently functionalized linkers with the same linkage and size. One is de novo synthesis by mixing the linkers during synthesis, where the anisotropy is introduced according to thermodynamic parameters of the reaction. The other is post-synthetic modification by replacing part of the existing linkers in MOFs with the new linkers, during which the spatial arrangements of the new functionalities are governed by the kinetics of the time-dependent exchange process.

Mixing linkers de novo

A straightforward method to obtain MTV-MOFs with functionality variance is to mix the components as starting materials through de novo synthesis. Here, we use MTV-MOF-5 as an example (FIG. 5a). BDC and its derivatives -NH_2, -Br, -$(Cl)_2$, -NO_2, -$(CH_3)_2$, -C_4H_4, -$(OC_3H_5)_2$ and -$(OC_7H_7)_2$ were used to synthesize 18 different types of MTV-MOF-5 structure[88]. Each type exhibits a unique combination of linkers with up to eight different functional groups in the same crystal. For each combination, the ratio between the functional groups can be continuously tuned, thus leading to the creation of an infinite number of new MOFs, each of which has a specific linker ratio. This MTV method not only enriched the variety of MOFs but also led to the creation of new pore and inner-surface environments within the framework[40,43,44,88,95,96]. Optimization of the pore environment in MTV-MOFs could be favourable for their

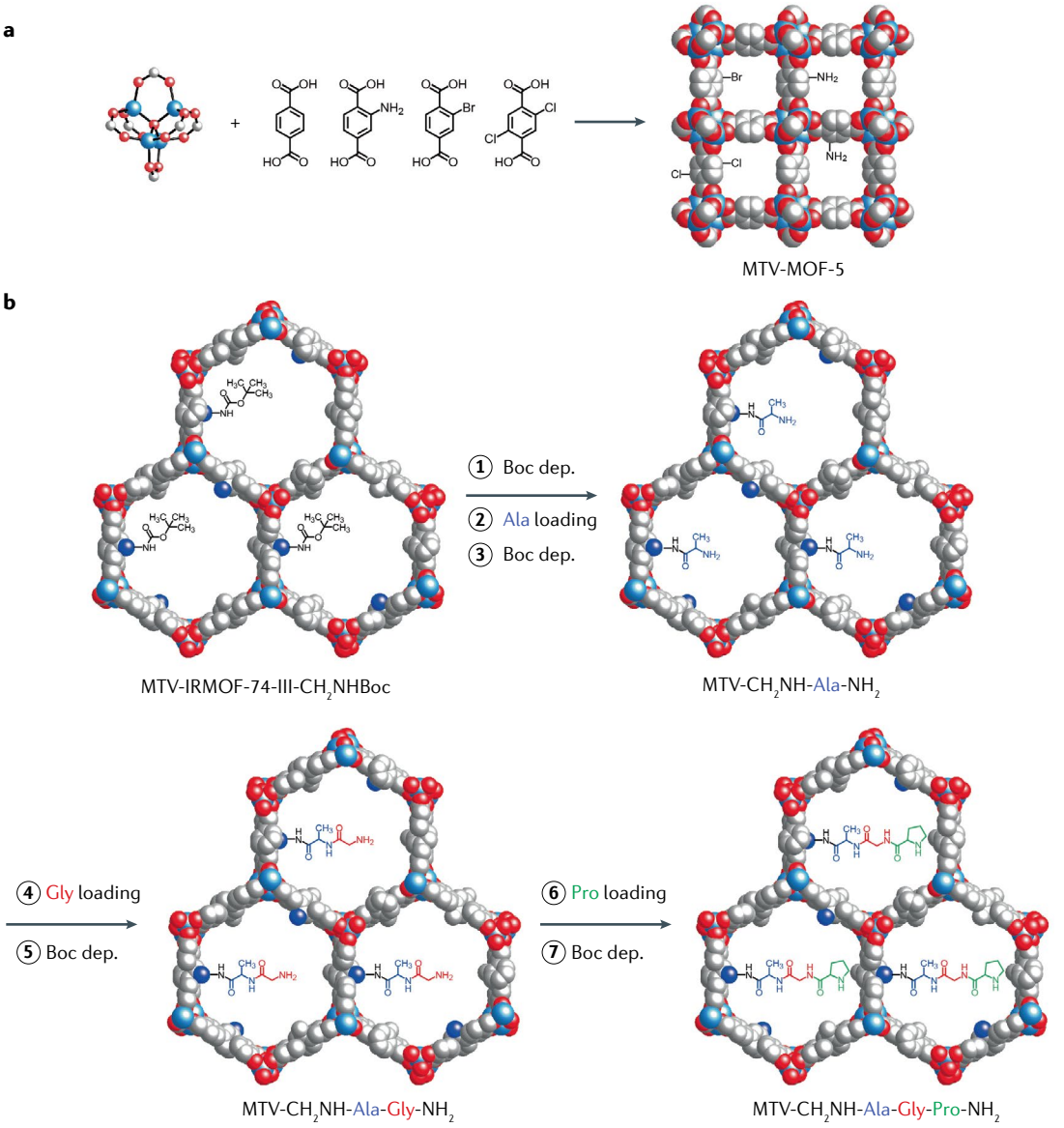

Fig. 5 | **Functionality variance in multivariate metal–organic frameworks (MTV-MOFs). a** | 1,4-Benzenedicarboxylate (BDC) and its derivatives are used to synthesize MTV-MOF-5 with functionality variance de novo[88]. **b** | By sequential post-synthetic modification, functionality variance is introduced into MTV-IRMOF-74-III (REF.[107]). Boc, *tert*-butoxylcarbonyl.

catalytic performance[97,98]. For instance, both activity and selectivity are adjusted by Pt-embedded MTV-UiO-66, where the $-NH_3^+$ functionalities influence the catalytic pathway, and strong acidic sites $-SO_3H$ tune the catalytic activity[97]. A synergistic effect between functionalities in MTV-MOF is also observed. Twenty-six MTV-UiO-66 frameworks, each with two mixed functionalities, are synthesized and tested for the degradation of a chemical warfare agent, 4-nitrophenylphosphate[98]. In terms of catalytic activity, several MTV-UiO-66 with mixed functionalities exceed physical mixtures of MOFs with only one corresponding functionality.

Another advantage of the MTV approach is the capability of continuously tuning the host–guest interaction within the pores endowed with multiple functional groups. In MIL-101 with two functionality variances, the percentage of each component is continuously tuned from 0% to 100% without altering the underlying topology[99]. In this way, the interaction between the resulting MTV-MIL-101 and the guest molecules (ibuprofen, rhodamine B and doxorubicin) is precisely tuned, as reflected in the quantitative control of their release rates. This MTV approach is not only applicable for dialling in the release behaviour of a specific drug but is also suited for programming the release profiles of multiple drugs simultaneously, which is desirable for personalized therapy[99]. Another example showing the advantage of continuous tuning in linker ratio is the achievement of cool white light by introducing red, green and blue fluorophores as functionality variance in Zr-MOF[100]. The emissive chromaticity of the MTV-MOFs is governed by the ratio of different fluorophores, obviating the inner filtering effect.

The most intriguing aspect of the MTV approach is the introduction of anisotropy into MOF crystals by the functional variance along a specific direction, plane or three-dimensional space. Positioning different linkers in the same MOF imparts new apportionment of functionalities to form large or small domains and alternating arrangement, in addition to random distribution[88,96]. These apportionments allow for improvements of 84% in H_2 storage capacity and 400% in CO_2 uptake for MTV-MOF-5 over the parent MOF-5 (REF.[88]). The generality of this observation is further supported by a 25% enhancement in H_2 uptake in an MTV-MOF-177 with functionality variance (-NH_2 and -OCH_3)[93], as well as a nonlinear correlation between the total volumetric CH_4 uptake and the percentage of terphenyl-3,3′,5,5′-tetracarboxylate (TPTC) in MTV-MOF UTSA-77–79 (REF.[101]).

Post-synthetic linker modification

Linker exchange represents another efficient way to achieve MTV-MOFs. Unlike the de novo approach, the spatial functionality arrangement is time-dependent during the post-synthetic modification, thus introducing an additional parameter for anisotropy. The functionality variance in the MOF is influenced by kinetic factors, such as the directionality of the linker diffusion and the exchange rate. Unless 100% conversion occurs, any intermediate state of linker exchange results in MTV-MOFs.

Linker exchange can be realized in many MOFs, including MIL-53(Al), MIL-68(In), ZIF-71, MIL-101-Cr, ZIF-8, MOF-5, UMCM-8 and UiO-66 under relatively mild conditions[102–105]. Sequential introduction of functionality variance (-Br and -NH_2) into MIL-101-Cr led to enhanced interaction with hydrogen for its storage in MOFs[103]. It is worth noting that linker exchange can also take place between linkers of different sizes. The BPDC linker in bio-MOF-100 is substituted stepwise by slightly longer linkers, azobenzene-4,4′-dicarboxylate (ABDC) and 2′-amino-1,1′-terphenyl-4,4′-dicarboxylate (NH_2-TPDC)[106]. After two consecutive linker exchanges, bio-MOF-103 is synthesized with 85% NH_2-TPDC and 15% ABDC.

MTV-MOFs obtained by de novo synthesis can be further modified by linker exchange to increase the overall functionality variance. MTV-IRMOF-74-III, MTV-$(CH_3)_{1-x}[CH_2NH\text{-}Boc]_x$ (Boc = *tert*-butyloxycarbonyl, $x = 0.2–0.8$), is functionalized by various peptides at the amine functionality through a covalent bond[107] (FIG. 5b). With up to seven steps of post-synthetic reactions, the same peptide sequence as in the active site of an enzyme (tobacco etch virus protease) is created in the MTV-MOF.

Metal variance and sequences

Metals are another class of important components in MOFs that can provide variances. There are three types of metal variance in MTV-MOF: variation of metals in SBUs, extraneous metals or metal clusters attached to the original SBUs and different metals inserted into linkers through coordination. In all these scenarios, the overall MOF geometry and the linkages between organic linkers and SBUs remain unaltered, and the anisotropy is originated from the ratio and spatial arrangement of metal components along specific directions of the crystal. Unlike the functionality variance in MTV-MOFs, where linkers with similar size are usually used, the construction of MTV-MOFs with multiple metals could involve metal or metal ions of different sizes, coordination geometry and strength. If such differences are not tolerated by the crystal lattice, usually a physical mixture of crystals with different compositions of metals, rather than MTV-MOFs, may form. In some cases, MOFs featuring definite heterometallic SBUs are possible[108]. In these MOFs, the types and positions of metals in the SBU can be molecularly defined by crystallography, because each metal has a characteristic coordination number and geometry and occupies crystallographically different sites. By definition, they are no longer considered as MTV-MOFs, because the ratio between the multiple metals cannot be varied.

Earlier than functionality variance, metal variance in MOFs was investigated in the search for customized MOF optical properties by introducing multiple types of metals, each having distinct fluorescence[109–112]. However, structural differences between MTV-MOFs and the physical mixtures of corresponding MOFs with single metal components were not revealed until the metal-coordination environments were studied in detail[113–115]. Spectroscopic methods suggest that the spatial arrangement of metal variance is neither linear nor random[116], because each SBU is composed of a unique combination of metals. The composition, directionality and spatial arrangement of SBUs contribute to the anisotropy of the MOF crystal, hence, the possible sequence across the framework. Indeed, the ratio of different metals in MTV-MOFs was found to deviate from the input metal ratio for MTV-MOFs synthesized using both the de novo method and post-synthetic modification[115–117]. This observation provides further evidence for the metal variance in MTV-MOFs and leads to the study of anisotropy in their crystal structures.

Mixing metals de novo

Similar to the introduction of functionality variance, the de novo method is also facile for the introduction of metal variance. Here, we use MTV-MOF-74 as an example[115], where up to ten kinds of different divalent metals, including Mg, Ca, Sr, Ba, Mn, Fe, Co, Ni, Zn and Cd, were incorporated into the structure of MOF-74 (FIG. 6a). The metal components in these MTV-MOFs were varied by gradual tuning of the stoichiometry in the starting materials. This metal variance in MTV-MOFs translates into their chemical stability, where introduction of either Ni^{2+} or Co^{2+} into Mg-MOF-74 at a certain ratio leads to the increase in their water stability[118]. Another useful feature of this approach is to incorporate a particular metal into MOFs that cannot be formed by using one metal alone, such as Ca, Sr and Ba for MTV-MOF-74. In another case, multiple metals (Co, Mn and Ca) are incorporated into the rod-shaped SBUs of ZnPF-1, where the sequence of the metals is controlled and deciphered[117].

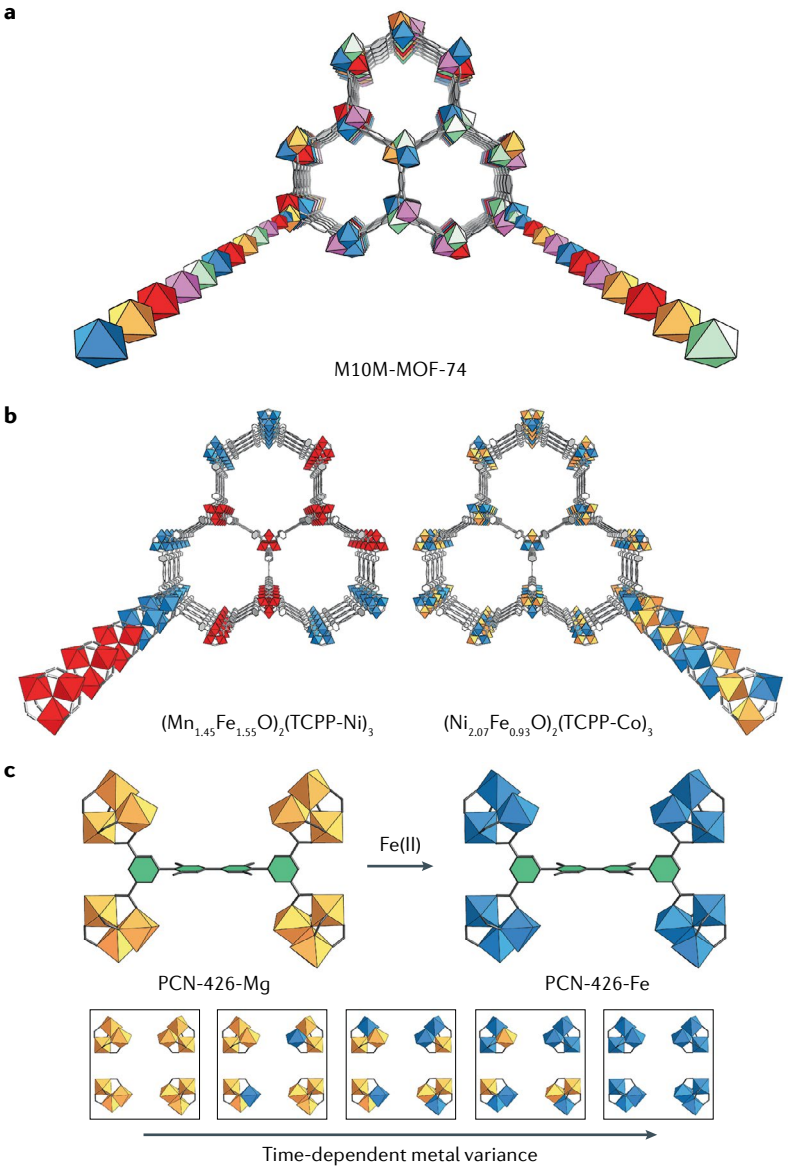

Fig. 6 | **Metal variance in multivariate metal–organic frameworks (MTV-MOFs).** **a** | Unique metal sequences are created in de novo synthesized MTV-MOF-74 as a result of metal variance[115]. **b** | Two kinds of spatial arrangement of metals are observed in two porphyrin-based MTV-MOFs creating different scenarios of metal variance. $(Mn_{1.45}Fe_{1.55}O)_2(TCPP\text{-}Ni)_3$ (TCPP = *tetrakis*(4-carboxyphenyl)porphyrin) (left) features domains with single-component $Mn_3(\mu_3\text{-}O)(COO)_6$ or $Fe_3(\mu_3\text{-}O)(COO)_6$ secondary building units. In contrast, $(Ni_{2.07}Fe_{0.93}O)_2(TCPP\text{-}Co)_3$ (right) has Ni^{2+} and Fe^{3+} well mixed in each secondary building unit[116]. **c** | By post-synthetic modification, PCN-426-Mg is gradually converted into PCN-426-Fe. Time-dependent metal variance is presented during the modification[125].

Introducing new metals to a known MOF brings additional metal variance to the usually inert structure. Through de novo synthesis, Co^{2+} is introduced into MOF-5 (up to 21%) to increase the H_2 uptake by 8%, owing to higher affinity of Co^{2+} to H_2 (REF.[119]). Similarly, CPM-200 exhibits enhanced CO_2 uptake by incorporating Mg^{2+} with open metal sites. By varying the metal combinations of trivalent (In^{3+}, Ga^{3+}, Fe^{3+}, V^{3+}, Sc^{3+}) and divalent (Mg^{2+}, Mn^{2+}, Co^{2+}, Ni^{2+}) metals, a correlation between the charge-to-radius ratio and isosteric heat for CO_2 is established, where CPM-200 with mixed V^{3+} and Mg^{2+} shows the highest isosteric heat (−79.6 kJ mol^{-1}) among them[120].

When two types of metals are introduced into one MTV-MOF, concerted operation is likely to be created. A typical example is cascade reactions using MTV-MOFs as catalysts, where each metal activates one particular step. MTV-MOFs with two or three M(salen)-derived linkers (M = Mn, Co, Fe, VO, Ru, Cu and Cr) are used in sequential epoxidation and ring-opening reactions of alkenes[121]. The MOF with Cu, Mn and Co mixed in the M(salen) units shows the best conversion and enantioselectivity, in which Mn^{3+} activates epoxidation of alkenes; Co^{3+} promotes the ring opening of epoxides; and Cu^{2+} is used to form interpenetrated structure ensuring close proximity between these catalytic sites.

Two forms of spatial arrangement, domains and well mixed, are observed in porphyrin-based MTV-MOFs with **stp** topology[116]. Specifically, $(Mn_{1.45}Fe_{1.55}O)_2(TCPP\text{-}Ni)_3$ (TCPP = *tetrakis*(4-carboxyphenyl)porphyrin) features domains with single-component $Mn_3(\mu_3\text{-}O)(COO)_6$ or $Fe_3(\mu_3\text{-}O)(COO)_6$ SBUs, and $(Ni_{2.07}Fe_{0.93}O)_2(TCPP\text{-}Co)_3$ with Ni^{2+} and Fe^{3+} mixing in each SBU (FIG. 6b). For the 1,5-dihydroxynaphthalene photo-oxidation reaction, different spatial arrangements in these MTV-MOFs result in different catalytic behaviour. $(Ni_{2.07}Fe_{0.93}O)_2(TCPP\text{-}Co)_3$ with well-mixed spatial arrangement of SBUs shows a 54% higher conversion rate than the physical mixture of MOFs with a single metal component.

Post-synthetic metalation

Sequential arrangement of metals can be introduced by temporal factors when post-synthetic modification is performed to make MTV-MOFs[122]. It has been shown that Cd^{2+} in a MOF, $Cd_{1.5}(H_3O)_3[(Cd_4O)_3(HETT)_8]\cdot 6H_2O$ (HETT = 5,5′,10,10′,15,15′-hexaethayltruxene-2,7,12-tricarboxylic acid), is exchangeable with Pb^{2+}, reversibly[123]. Complete replacement can be achieved here, while MTV-MOFs are formed during the process. Compared with the exchange with metals of the same valance, the exchange with metals of different valence is more challenging. Incomplete replacement is usually observed as shown in the case of MOF-5(Zn^{2+}) immersed in Ti^{3+}, V^{3+} and Cr^{3+} with partial replacement[124]. In the study of PCN-426-Mg (REF.[125]) (FIG. 6c), Mg^{2+} is substituted first with divalent metal ions (Fe^{2+}, Cr^{2+}) to achieve complete conversion. Then, these metals are oxidized to yield MOFs with trivalent metal ions (Fe^{3+}, Cr^{3+}), achieving much faster kinetics in comparison with direct exchange with trivalent metal ions. During both exchange and oxidation processes, MTV-MOFs with metal variance (in metal type and charge) is inevitable. It is noticeable that the formation of different domains with single metals as in de novo synthesis, rather than mixing different metals in each SBU, has yet to be demonstrated using post-synthetic modification.

Metal variance can also be achieved by inserting various metals into the linkers or replacing a metal-free linker with a metal-coordinated linker. A typical example is the insertion of Pd^{2+} and Cu^{2+} into the open 2,2′-bipyridine sites in MOF-253, and enhanced selectivity for the adsorption of CO_2 over N_2 is observed[126]. Different metals are incorporated into Zr-based chiral

UiO-68 constructed by salen linker by post-synthetic exchange[127]. The resulting MTV-MOFs are efficient for a range of asymmetric organic reactions, such as asymmetric epoxidation of alkenes, cyanosilylation of aldehydes and aminolysis of *trans*-stilbene. Moreover, the MTV-UiO-68 with Mn and Cr can catalyse a sequential reaction of epoxidation and ring-opening reaction.

In addition to metal variance in SBUs, and in linkers anchored by coordination bonds, a third type of metal variance, extraneous metals or metal clusters attached to the original SBUs, can be achieved by post-synthetic modification. In Zr-based MOFs, V^{5+}, In^{3+}, Al^{3+}, Mg^{2+}, Co^{2+}, Cu^{+} and Li^{+} can be attached to their SBUs by coordinating with one or more oxygen atoms[128–132]. It is worth noting that not all of these oxygen atoms are coordinated with the extraneous metals. The positions of extraneous metals in each SBU cannot be distinguished by crystallography, therefore, these MOFs are, indeed, MTV-MOFs. The resulting metal variance alters the chemical environment around SBUs without replacing the original metals, as shown in the favoured catalytic reactions, including borylation, silylation, amination, olefin hydrogenation[130], as well as hydrogenation of nitroarenes, nitriles and isocyanides species[131].

When more than one kind of extraneous metal is attached to the same SBU, the anisotropy of the MOF is further increased, leading to a more sophisticated tuning of the catalytic activity[23]. In a Zr-based MOF with triphenyldicarboxylic acid, 11 Cu^{+} and 3 Li^{+} are simultaneously introduced into the same $Zr_{12}O_8(\mu_3\text{-}OH)_8(\mu_2\text{-}OH)_6(CO_2)_{18}$ SBU, where Cu^{+} is the active site for efficient CO_2 conversion into ethanol and Li^{+} stabilizes the reaction intermediate. The positions of extraneous metals on SBUs are shown to be critical for the overall catalytic performance[130], further outlining the importance of the control of anisotropy in MOFs.

Mapping the spatial arrangements

In contrast to multinary MOF structures where the variance is in the backbone, the variances in organic functionality or metal share the same crystallographic sites within the corresponding MTV-MOFs. Consequently, these components become crystallographically indistinguishable. Moreover, vacancies in the MOFs are usually viewed as backbones with lower occupancies statistically, and their locations are not precisely defined. While deciphering their spatial arrangements is a challenge, numerous efforts have been made to characterize functionality and metal variances and vacancies in MOFs, and a number of techniques have been developed over recent years[94]. Here, we group them into three categories based on the type of component: linkers, metals and their vacancies.

Spatial arrangement of linkers

Solid-state nuclear magnetic resonance (NMR) spectroscopy has proven to be an effective tool to characterize the average distances and distributions of linkers or linker domains within MTV-MOFs. In MTV-MOF-5, up to eight different linkers can be incorporated into one single crystal without causing phase separation. ^{13}C–^{15}N rotational-echo double-resonance NMR spectroscopy was applied to isotopically labelled MTV-MOF-5 systems to study the functionality variance and sequence[96]. In the rotational-echo double-resonance method, the decay rate of the dipolar coupling between ^{13}C and ^{15}N is correlated with the interdistance of linkers, and a fast decay translates to a close proximity between the linkers. Combined with computational modelling, several unique patterns, including small clustering, random and alternating arrangements were discovered for MTV-MOF-5 systems with different functionality variance. Arrangement patterns on MTV-MOF-5 structures with up to three different functionalities were obtained with high confidence.

Other NMR spectroscopy techniques based on ^{1}H solid-state NMR spectroscopy on non-labelled linkers provide more accessible alternatives to study the functionality variance in MTV-MOF structures. Homogeneous linker distribution of two linkers with equal lengths, BPDC and bipyridyl dicarboxylic acid (BPyDC), was found in DUT-5 using ^{1}H spin-diffusion NMR spectroscopy[133], and linker clustering was evidenced through ^{1}H combined rotation and multiple-pulse NMR spectroscopy in mixed-linker ZIF-8_x-90_{1-x} (REF. [134]).

Optical imaging, while limited in resolution, was also found to provide information on functionality variance in MTV systems. MTV-UiO-67 with two different dye-functionalized linkers was analysed by fluorescence imaging and lifetime analysis[135]. The spatial arrangement of functionalities and the level of defects were imaged for single crystals and polycrystalline samples. The fluorescence imaging and lifetime analysis showed that homogeneous distribution of functionalities was found in both cases, while MTV-UiO-67 synthesized by post-synthetic modification contains fewer defects compared with that by de novo synthesis.

Spatial arrangement of metals

The spatial arrangement of metals in MTV-MOFs can be deciphered over different length scales, depending on the techniques. Occasionally, surface X-ray diffraction can be used to extract sequential information from MTV-MOFs; however, this technique is generally limited to simple and repeating sequences of metal ions[117]. In a series of mixed-metal MOFs based on ZnPF-1, several kinds of metal ions with tetrahedral coordination occupy crystallographically equivalent sites within the infinite-rod SBU. Interestingly, when the crystal is cooled down below 50 K, half of the tetrahedral metal sites become octahedral coordinated, transforming the two adjacent sites from equivalent to crystallographically distinguishable, thus revealing an alternating metal sequence along the rod SBU. The octahedral metal site is found to be a mixed-metal site of Mn^{2+}, Co^{2+} or Ca^{2+}, while the tetrahedral site accommodates Zn^{2+} or Co^{2+}. Although the information provided by surface X-ray diffraction is still not enough to solve the exact sequence of metal ions, it narrows down the possibilities of the metal-ion arrangement along the rod SBU.

X-ray photoelectron spectroscopy (XPS) also provides indirect information on the spatial arrangement of metals inside MOFs. Local environment

differences of the metals are reflected in their respective signature photoelectron energy. In mixed-metal $[M_3(\mu_3\text{-}O)]_2(TCPP\text{-}M)_3$ (M = Mn, Fe, Ni), different metal ions can either be well mixed within the $M_3(\mu_3\text{-}O)(COO)_6$ SBUs or distributed in respective single-component SBU manner. Through XPS, it was found that the $2p_{3/2}$ peak of the metals in mixed-metal $M_3(\mu_3\text{-}O)(COO)_6$ SBU is slightly shifted with respect to its single-component counterparts[116]. Compared with MOFs with pure Ni^{2+} or Fe^{3+}, shifts of 0.2 eV and 0.5 eV, respectively, were observed, showing the mixing of Ni^{2+} and Fe^{3+} within the trimetallic SBU.

Although MOF–nanoparticle hybrid structures are not covered in this Review, it is useful to know that surface-enhanced Raman spectroscopy (SERS) was employed to image the distribution of metal-containing linkers in an MTV-MOF–nanoparticle hybrid system with mesoscopic resolution[136]. Specifically, silver nanoparticles were enclosed in an oriented MTV-MOF shell with controllable thickness to form hybrid structures with plasmonic activities. The distribution of metalated and unmetalated porphyrin linkers in the MOF shell was clearly imaged through SERS, and a uniform distribution of the metalated linkers throughout the MOF was observed.

Observation of vacancies in backbones

X-ray techniques, including diffuse scattering, anomalous X-ray scattering and pair distribution function measurements, were used to detect vacancies in UiO-66(Hf)[73]. The ordered **reo** defects were first discovered in UiO-66(Hf) by analysing diffuse scattering from superlattice peaks. The ordered missing-SBU vacancies were further confirmed by comparing the anomalous X-ray scattering pattern measured away from and on the Hf K-absorption edge.

Recently, high-resolution transmission electron microscopy (HRTEM) was developed as a powerful tool to directly observe structural vacancies in MOFs with atomic resolution. UiO-66 has been widely investigated as a model system for analysis because of its high concentration of vacancies under certain synthetic protocols. Compared with conventional HRTEM, the combination of a low-dose HRTEM technique and electron crystallography overcomes the challenge of beam damage, revealing sub-nanometre structural details of UiO-66 that were previously unknown[74]. Through contrast transfer function corrected HRTEM analysis, both the SBUs and the linkers showed different contrast with the pore environment, and, thus, can be directly observed in real space. Based on the HRTEM images obtained, both missing-linker and missing-SBU defects were found in UiO-66. Specifically, **reo** defects, as well as the previously unreported **scu** domains, were observed in UiO-66 at the same time. It was also found that missing-SBU domains are only a few unit cells in dimension, while missing-linker domains with long-range order over multiple unit cells have been observed. Although HRTEM has not yet been applied to MTV-MOF structures, it holds promise in unveiling sequences of metals and linkers in a variety of different scenarios.

Directional motion and dynamics in MOFs

Different strategies have been described with which anisotropy can be introduced into or imposed onto the ordered backbone of MOFs. All aforementioned cases can be classified as static anisotropy where, variance in composition along a specific direction is constant and does not change over time. In contrast, in the case of dynamic anisotropy, the composition of the structure changes continuously because of large-amplitude motion of its constituents' dynamics[137–139]. Anisotropy introduced according to this approach is unique in that sequences change over the course of time.

Two approaches have been devised with which dynamic motion can be achieved within the confines of the ordered backbone of MOFs: global dynamics, where the backbone is dynamic[18,140–142], and local dynamics, where the motion is independent of the framework's backbone[143,144]. In the context of anisotropic reticular chemistry, we will only consider the latter case because the existence of an ordered backbone with respect to which anisotropy is introduced into the system is fundamental to the concept of this contribution. Anisotropy in dynamic frameworks is manifested in two ways: sequences of constituents that move independently, thus creating unique interconverting sequences of functionality or the motion itself can be anisotropic when the constituents move in a synchronized manner and along a specified direction. Notably, in this latter case, the order of the system does not decrease, despite a net input of energy. As such, it can be classified as a special case of non-equilibrium (dynamic) self-assembly[145]. Finally, the incorporation of dynamic modules into the ordered backbone of MOFs can be achieved by covalently appending photoswitches, as well as by mechanically entangling molecular species. Illustrative examples for both are highlighted in the following sections.

Anisotropy with covalent functions

Two-state dynamics of appended photoswitches. The most investigated approach towards introducing dynamics into MOFs is to append photoswitchable functional groups onto the ordered backbone of a framework. A variety of different photoswitches can be incorporated according to this strategy[146–148] (FIG. 7a). For instance, azobenzene moieties can be dangled into the pores of IRMOF-74-III, where, upon irradiation with light of a specific wavelength (408 nm), this moiety exhibits a wagging motion, owing to repetitive isomerization from its *cis* to its *trans* configuration[149]. As such, the respective orientation of *cis* and *trans* azobenzene functionalities in the pores with respect to each other is changing constantly, and an infinite number of unique interconverting sequences are present at any given point in time. The azobenzene moiety allows for facile chemical modification and, thus, in theory, for multivariate functionalization to further increase the complexity of the resulting system.

Continuous anisotropic motion of a molecular rotor. motors[150] (FIG. 7b). These motors use light and heat to carry out unidirectional rotation; each 360° cycle is affected by two photochemical *E*/*Z* isomerization steps,

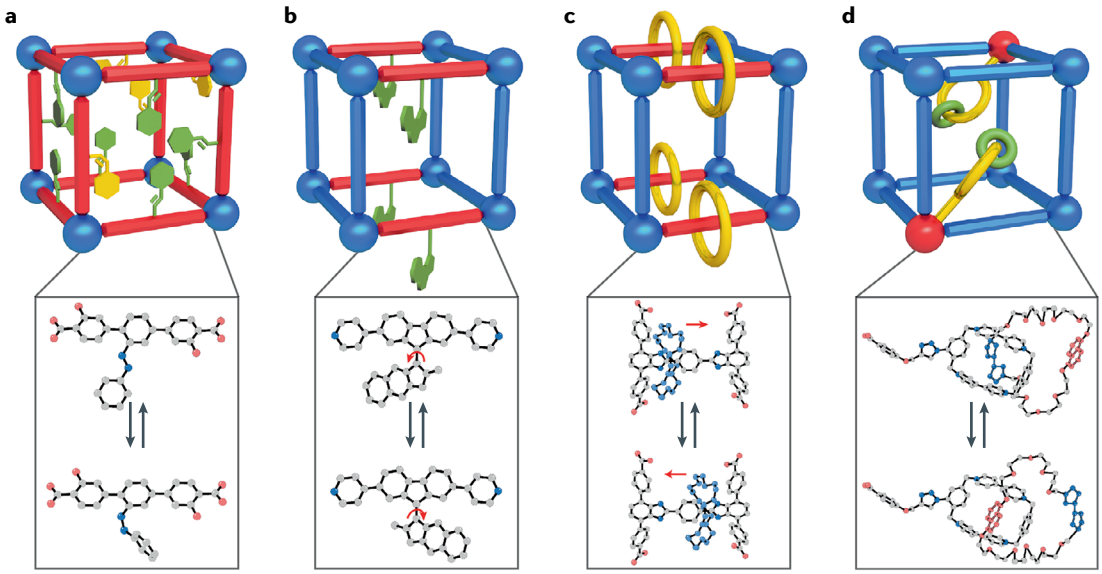

Fig. 7 | **Different modes of anisotropic motion in metal–organic frameworks. a** | Dynamic anisotropy by appended photoswitches on the backbone of the framework[149]. **b** | Continuous anisotropic motion of covalently attached molecular rotors[150]. **c** | Dynamic anisotropy of molecular shuttles based on mechanical entanglement[151]. **d** | Anisotropic motion of bistable catenated rings mechanically interlocked with the framework backbone[152].

followed by a thermally driven helix inversion. In the structure of moto-MOF1, the struts are aligned with respect to one another and, upon exposure to the photochemical and thermal stimuli, rotate in an ordered and synchronized manner. Notably, the high anisotropy of this motion is enabled by both the unidirectional rotation and also by the spatial organization of the rotors, which are aligned parallel to one another in the crystal structure.

Anisotropy with mechanical interlocking

Two-state dynamics in a MOF molecular shuttle. In UWDM-4, 18-crown-6 ether macrocycles are spatially confined to the crossbars between two triphenyldicarboxylic acids of the MOFs[151] (FIG. 7c). The macrocycle is not chemically bound to the linker and is only held in place through mechanical entanglement. Consequently, the motion of the ring at room temperature is not restricted. The electron-rich macrocycle interacts strongly with the two spatially separated electron-poor imidazole moieties of the crossbar and, at room temperature, shuttles between them continuously. This motion is corroborated by variable-temperature solid-state NMR spectroscopy data, where only one resonance structure is detected for occupied and unoccupied imidazole moieties on an NMR spectroscopy timescale. When the temperature is decreased, the motion is slowed down and two distinct imidazole signals (occupied and unoccupied) can be observed.

Anisotropic motion of a bistable MOF catenane. To exert more control over the motion of mechanically appended functionality, a bistable interlocked molecule was introduced into NU-1000 according to a post-synthetic modification protocol (FIG. 7d). Owing to the steric demand of the bistable [2]catenane, an average of two out of the six possible struts of NU-1000 can be replaced by the functionalized linker[152]. The redox-active [2]catenane is comprised of a tetracationic cyclo(bisparaquat-*p*-phenylene) macrocycle, which mechanically interlocks with a macrocyclic polyether bearing both an electron-rich tetrathiafulvalene and a 1,5-dioxynaphthalene recognition site. The tetrathiafulvalene moiety can be oxidized and reduced by cyclic voltammetry. In the reduced state, the tetrathiafulvanene group interacts more favourably with cyclo(bisparaquat-*p*-phenylene). However, upon oxidation, electronic repulsion leads to rotation of the rings with respect to each other, such that the 1,5-dioxynaphthalene moiety interacts with the tetracationic macrocycle. Evidence for the motion within the confines of NU-1000 is found in solid-state UV–vis–NIR reflectance spectroscopy and cyclic voltammetry. It must be pointed out that, while there are only two distinct states that can be accessed in a controlled fashion, the rotation of the rings throughout the framework is not unidirectional, thus limiting the anisotropy of this dynamic process.

Outlook

Considering the current state of synthetic materials and how far molecular chemistry has evolved in its sophistication and precision, one is struck by how relatively 'primitive' synthetic materials are in their structures and functions. The chemical structures of materials are either too simple to carry out complex operations or too complex and chaotic to characterize and decipher how they operate. Reticular structures have bridged this gap because, like molecules, they can be designed with precision, and our ability to make them in crystalline form vastly contributes to correlating the structure and functionality. In other words, the two advantages that reticular chemistry offers are the ability to design in

infinite two and three dimensions, and the obtainment of these designs in crystalline form that can be definitively characterized at the atomic level. This reticular platform has been developed to make MOFs where their synthesis and structural characterization are now well-established science, and the facility with which their pores can be modified is beginning to be fruitfully applied in targeting specific properties. More exactly, MOFs are starting to show the way for increasing materials' complexity without falling into the chaos that comes with incorporating synthetic complexity.

We expect that dividing the frameworks into backbone and functionality constitutes the first conceptual step in bringing order to complexity. This concept can be explained in the following way: the order imparted by the MOF backbone is not altered when it is functionalized by an organic or a metal-coordinating group, or, better yet and more to the point, many different kinds of such groups. The variety of groups bound to the backbone and their spatial arrangements, when considered alone, may seem chaotic and random, but their strong binding to the backbone means that they are at least metrically defined. The distance between them is governed by their 'pinning' positions onto the backbone, which, fortunately, is ordered. Therefore, metrically, these multiple functionalities are well defined, and so are their identity and character. The system we just described is complex but the complexity is tied to order, distinguishing this construct from one where multiple functionalization causes fundamental change to the overall structure and leads to chaos and lack of crystallinity, such as that often found in polymers.

When the pinned complexity is coupled to the variation one makes in the backbone itself, such as using multiple building blocks to reticulate it, we achieve the fullness of complexity in MOFs. The variety of building units that can be deployed in the backbone and their arrangements lead to backbone variance, while the variety of organic functionalities that can be attached to that backbone and their spatial arrangements lead to functionality variance. In addition, the arrangement of various metals within each building unit leads to metal variance. The future of MOFs lies in how we can design these variances and how to describe them. We propose that, in the fullness of time, these variances will follow unique sequences and that these sequences will encompass a variety of properties, such as what we described in this Review in terms of anisotropy. This unique property pertains to the infinite chemical information in the pores and within the backbones of MOFs. We anticipate that the consummate MOF in future will have unique sequences describing its backbone variance joined to unique sequences that describe its functionality and metal variance. These sequences are able to work synergistically to perform not just one operation but many operations in series or in parallel. Anisotropy built into these sequences ensures directionality in controlling how molecules pass through the pores and the circuitry that they may follow in permeating the MOF.

What we have just described is an infinite chemistry, which is no longer limited by chaos caused by the introduction of complexity but, rather, enhanced by it, as is the case in biological systems. We are witnessing the very early stages of being able to concept transfer from biology (though not mimicking) with a sophistication far exceeding any experienced in synthetic materials thus far. Accordingly, we should be able to make MOF systems that are entirely regulated and operated by sequences of chemical information. It should be possible to make structures having compartments that are linked together and open to each other, yet, operating independently. It is not unreasonable to anticipate MOFs capable of sorting and counting incoming molecules, with the ability to vary and control the kinetics of such operations within one structure. The concepts of anisotropic reticular chemistry, including the complexity of sequences, have the power of transforming our view of synthetic materials and, indeed, our way of making and using them. Obviously, these developments will require characterization methods to be invented in order to catch up with the sophistication of incorporating sequences within MOFs. However, because the materials we describe in this Review, under the umbrella of anisotropic reticular chemistry, and their variations can be prepared in a controlled and designed manner, we will not be short of substances to examine in certain ranges of properties and to correlate their observed behaviour with theoretically expected sequences. Clearly, the power of anisotropic reticular chemistry is inevitably linked to big data, machine learning and artificial intelligence tools to solve what promises to be the materials problem of the century.

Published online: 13 August 2020

1. Yaghi, O. M., Kalmutzki, M. J. & Diercks, C. S. *Introduction to Reticular Chemistry: Metal-Organic Frameworks and Covalent Organic Frameworks* (Wiley, 2019).
2. Furukawa, H., Cordova, K. E., O'Keeffe, M. & Yaghi, O. M. The chemistry and applications of metal–organic frameworks. *Science* **341**, 1230444 (2013).
3. Kalmutzki, M. J., Hanikel, N. & Yaghi, O. M. Secondary building units as the turning point in the development of the reticular chemistry of MOFs. *Sci. Adv.* **4**, eaat9180 (2018).
4. Li, H., Eddaoudi, M., Groy, T. L. & Yaghi, O. M. Establishing microporosity in open metal–organic frameworks: gas sorption isotherms for Zn(BDC) (BDC = 1,4-benzenedicarboxylate). *J. Am. Chem. Soc.* **120**, 8571–8572 (1998).
5. Li, H., Eddaoudi, M., O'Keeffe, M. & Yaghi, O. M. Design and synthesis of an exceptionally stable and highly porous metal–organic framework. *Nature* **402**, 276–279 (1999).
6. Park, K. S. et al. Exceptional chemical and thermal stability of zeolitic imidazolate frameworks. *Proc. Natl Acad. Sci. USA* **103**, 10186–10191 (2006).
7. Banerjee, R. et al. High-throughput synthesis of zeolitic imidazolate frameworks and application to CO_2 capture. *Science* **319**, 939–943 (2008).
8. Kitagawa, S., Kitaura, R. & Noro, S. Functional porous coordination polymers. *Angew. Chem. Int. Ed.* **43**, 2334–2375 (2004).
9. Férey, G. Hybrid porous solids: past, present, future. *Chem. Soc. Rev.* **37**, 191–214 (2008).
10. Zhang, J.-P., Zhang, Y.-B., Lin, J.-B. & Chen, X.-M. Metal azolate frameworks: from crystal engineering to functional materials. *Chem. Rev.* **112**, 1001–1033 (2012).
11. Gonzalez, M. I. et al. Confinement of atomically defined metal halide sheets in a metal–organic framework. *Nature* **577**, 64–68 (2019).
12. Li, L. et al. Ethane/ethylene separation in a metal–organic framework with iron-peroxo sites. *Science* **362**, 443–446 (2018).
13. Chen, K.-J. et al. Synergistic sorbent separation for one-step ethylene purification from a four-component mixture. *Science* **366**, 241–246 (2019).
14. Li, P. et al. Bottom-up construction of a superstructure in a porous uranium-organic crystal. *Science* **356**, 624–627 (2017).
15. Gu, C. et al. Design and control of gas diffusion process in a nanoporous soft crystal. *Science* **363**, 387–391 (2019).
16. Liu, G. et al. Mixed matrix formulations with MOF molecular sieving for key energy-intensive separations. *Nat. Mater.* **17**, 283–289 (2018).
17. Fateeva, A. et al. A water-stable porphyrin-based metal–organic framework active for visible-light photocatalysis. *Angew. Chem. Int. Ed.* **51**, 7440–7444 (2012).

18. Krause, S. et al. A pressure-amplifying framework material with negative gas adsorption transitions. *Nature* **532**, 348–352 (2016).
19. Boyd, P. G. et al. Data-driven design of metal–organic frameworks for wet flue gas CO_2 capture. *Nature* **576**, 253–256 (2019).
20. Lo, S.-H. et al. Rapid desolvation-triggered domino lattice rearrangement in a metal–organic framework. *Nat. Chem.* **12**, 90–97 (2020).
21. Yan, Y. et al. Metal–organic polyhedral frameworks: high H_2 adsorption capacities and neutron powder diffraction studies. *J. Am. Chem. Soc.* **132**, 4092–4094 (2010).
22. Liao, P.-Q., Huang, N.-Y., Zhang, W.-X., Zhang, J.-P. & Chen, X.-M. Controlling guest conformation for efficient purification of butadiene. *Science* **356**, 1193–1196 (2017).
23. Cao, L. et al. Self-supporting metal–organic layers as single-site solid catalysts. *Angew. Chem. Int. Ed.* **55**, 4962–4966 (2016).
24. Sheberla, D. et al. Conductive MOF electrodes for stable supercapacitors with high areal capacitance. *Nat. Mater.* **16**, 220–224 (2016).
25. Farha, O. K. et al. Metal–organic framework materials with ultrahigh surface areas: is the sky the limit? *J. Am. Chem. Soc.* **134**, 15016–15021 (2012).
26. Hwang, Y. K. et al. Amine grafting on coordinatively unsaturated metal centers of MOFs: consequences for catalysis and metal encapsulation. *Angew. Chem. Int. Ed.* **47**, 4144–4148 (2008).
27. Rodenas, T. et al. Metal–organic framework nanosheets in polymer composite materials for gas separation. *Nat. Mater.* **14**, 48–55 (2015).
28. Zhao, M. et al. Metal–organic frameworks as selectivity regulators for hydrogenation reactions. *Nature* **539**, 76–80 (2016).
29. Nugent, P. et al. Porous materials with optimal adsorption thermodynamics and kinetics for CO_2 separation. *Nature* **495**, 80–84 (2013).
30. Zhai, Q.-G. et al. An ultra-tunable platform for molecular engineering of high-performance crystalline porous materials. *Nat. Commun.* **7**, 13645 (2016).
31. Sun, C.-Y. et al. Efficient and tunable white-light emission of metal–organic frameworks by iridium-complex encapsulation. *Nat. Commun.* **4**, 2717 (2013).
32. Mo, K., Yang, Y. & Cui, Y. A homochiral metal–organic framework as an effective asymmetric catalyst for cyanohydrin synthesis. *J. Am. Chem. Soc.* **136**, 1746–1749 (2014).
33. McHugh, L. N. et al. Hydrolytic stability in hemilabile metal–organic frameworks. *Nat. Chem.* **10**, 10960–11102 (2018).
34. Cui, X. et al. Pore chemistry and size control in hybrid porous materials for acetylene capture from ethylene. *Science* **353**, 141–144 (2016).
35. Taylor, J. M. et al. Facile proton conduction via ordered water molecules in a phosphonate metal–organic framework. *J. Am. Chem. Soc.* **132**, 14055–14057 (2010).
36. Horcajada, P. et al. Porous metal–organic-framework nanoscale carriers as a potential platform for drug delivery and imaging. *Nat. Mater.* **9**, 172–178 (2010).
37. Bloch, W. M. et al. Capturing snapshots of post-synthetic metallation chemistry in metal–organic frameworks. *Nat. Chem.* **6**, 906–913 (2014).
38. Dong, R. et al. High-mobility band-like charge transport in a semiconducting two-dimensional metal–organic framework. *Nat. Mater.* **17**, 1027–1032 (2018).
39. Bennett, T. D. et al. Melt-quenched glasses of metal–organic frameworks. *J. Am. Chem. Soc.* **138**, 3484–3492 (2016).
40. Feng, L., Wang, K.-Y., Day, G. S. & Zhou, H.-C. The chemistry of multi-component and hierarchical framework compounds. *Chem. Soc. Rev.* **48**, 4823–4853 (2019).
41. Furukawa, S., Reboul, J., Diring, S., Sumida, K. & Kitagawa, S. Structuring of metal–organic frameworks at the mesoscopic/macroscopic scale. *Chem. Soc. Rev.* **43**, 5700–5734 (2014).
42. Pang, Q., Tu, B. & Li, Q. Metal–organic frameworks with multicomponents in order. *Coord. Chem. Rev.* **388**, 107–125 (2019).
43. Jiao, J., Gong, W., Wu, X., Yang, S. & Cui, Y. Multivariate crystalline porous materials: Synthesis, property and potential application. *Coord. Chem. Rev.* **385**, 174–190 (2019).
44. Furukawa, H., Müller, U. & Yaghi, O. M. "Heterogeneity within order" in metal–organic frameworks. *Angew. Chem. Int. Ed.* **54**, 3417–3430 (2015).
45. Chevreau, H. et al. Mixed-linker hybrid superpolyhedra for the production of a series of large-pore iron(III) carboxylate metal–organic frameworks. *Angew. Chem. Int. Ed.* **52**, 5056–5060 (2013).
46. Jiang, H. et al. Enriching the reticular chemistry repertoire: merged nets approach for the rational design of intricate mixed-linker metal–organic framework platforms. *J. Am. Chem. Soc.* **140**, 8858–8867 (2018).
47. Kondo, M. et al. Rational synthesis of stable channel-like cavities with methane gas adsorption properties: $[\{Cu_2(pzdc)_2(L)\}_n]$ (pzdc = pyrazine-2,3-dicarboxylate; L = a pillar ligand). *Angew. Chem. Int. Ed.* **38**, 140–143 (1999).
48. Dybtsev, D. N., Chun, H. & Kim, K. Rigid and flexible: a highly porous metal–organic framework with unusual guest-dependent dynamic behavior. *Angew. Chem. Int. Ed.* **116**, 5145–5146 (2004).
49. Farha, O. K., Malliakas, C. D., Kanatzidis, M. G. & Hupp, J. T. Control over catenation in metal–organic frameworks via rational design of the organic building blocks. *J. Am. Chem. Soc.* **132**, 950–952 (2010).
50. Koh, K., Wong-Foy, A. G. & Matzger, A. J. A crystalline mesoporous coordination copolymer with high microporosity. *Angew. Chem. Int. Ed.* **47**, 677–680 (2008).
51. Koh, K., Wong-Foy, A. G. & Matzger, A. J. A porous coordination copolymer with over 5000 m^2/g BET surface area. *J. Am. Chem. Soc.* **131**, 4184–4185 (2009).
52. Koh, K., Wong-Foy, A. G. & Matzger, A. J. Coordination copolymerization mediated by $Zn_4O(CO_2R)_6$ metal clusters: a balancing act between statistics and geometry. *J. Am. Chem. Soc.* **132**, 15005–15010 (2010).
53. Furukawa, H. et al. Ultrahigh porosity in metal–organic frameworks. *Science* **329**, 424–428 (2010).
54. Klein, N. et al. A mesoporous metal–organic framework. *Angew. Chem. Int. Ed.* **48**, 9954–9957 (2009).
55. Hönicke, I. M. et al. Balancing mechanical stability and ultrahigh porosity in crystalline framework materials. *Angew. Chem. Int. Ed.* **57**, 13780–13783 (2018).
56. Liu, L., Konstas, K., Hill, M. R. & Telfer, S. G. Programmed pore architectures in modular quaternary metal–organic frameworks. *J. Am. Chem. Soc.* **135**, 17731–17734 (2013).
57. Liu, L., Zhou, T.-Y. & Telfer, S. G. Modulating the performance of an asymmetric organocatalyst by tuning its spatial environment in a metal–organic framework. *J. Am. Chem. Soc.* **139**, 13936–13943 (2017).
58. Liang, C.-C. et al. Engineering of pore geometry for ultrahigh capacity methane storage in mesoporous metal–organic frameworks. *J. Am. Chem. Soc.* **139**, 13300–13303 (2017).
59. Wong-Foy, A. G., Lebel, O. & Matzger, A. J. Porous crystal derived from a tricarboxylate linker with two distinct binding motifs. *J. Am. Chem. Soc.* **129**, 15740–15741 (2007).
60. Nouar, F. J. et al. Supermolecular building blocks (SBBs) for the design and synthesis of highly porous metal-organic frameworks. *J. Am. Chem. Soc.* **130**, 1833–1835 (2008).
61. Tu, B. et al. Heterogeneity within a mesoporous metal–organic framework with three distinct metal-containing building units. *J. Am. Chem. Soc.* **137**, 13456–13459 (2015).
62. Tu, B. et al. Reversible redox activity in multicomponent metal–organic frameworks constructed from trinuclear copper pyrazolate building blocks. *J. Am. Chem. Soc.* **139**, 7998–8007 (2017).
63. Liu, Q. et al. Mesoporous cages in chemically robust MOFs created by a large number of vertices with reduced connectivity. *J. Am. Chem. Soc.* **141**, 488–496 (2019).
64. Tu, B. et al. Harnessing bottom-up self-assembly to position five distinct components in an ordered porous framework. *Angew. Chem. Int. Ed.* **58**, 5348–5353 (2019).
65. Schaate, A. et al. Modulated synthesis of Zr-based metal–organic frameworks: from nano to single crystals. *Chem. Eur. J.* **17**, 6643–6651 (2011).
66. Trickett, C. A. et al. Definitive molecular level characterization of defects in UiO-66 crystals. *Angew. Chem. Int. Ed.* **54**, 11162–11167 (2015).
67. Fu, Y. et al. Duet of acetate and water at the defects of metal–organic frameworks. *Nano Lett.* **19**, 1618–1624 (2019).
68. Fang, Z., Bueken, B., De Vos, D. E. & Fischer, R. A. Defect-engineered metal–organic frameworks. *Angew. Chem. Int. Ed.* **54**, 7234–7254 (2015).
69. Wang, Y., Liu, Q., Zhang, Q., Peng, B. & Deng, H. Molecular vise approach to create metal-binding sites in MOFs and detection of biomarkers. *Angew. Chem. Int. Ed.* **57**, 7120–7125 (2018).
70. Yang, S. et al. A partially interpenetrated metal–organic framework for selective hysteretic sorption of carbon dioxide. *Nat. Mater.* **11**, 710–716 (2012).
71. Choi, K. M., Jeon, H. J., Kang, J. K. & Yaghi, O. M. Heterogeneity within order in crystals of a porous metal–organic framework. *J. Am. Chem. Soc.* **133**, 11920–11923 (2011).
72. Liu, Y. & Tang, Z. Multifunctional nanoparticle@MOF core–shell nanostructures. *Adv. Mater.* **25**, 5819–5825 (2013).
73. Cliffe, M. J. et al. Correlated defect nanoregions in a metal–organic framework. *Nat. Commun.* **5**, 4176 (2014).
74. Liu, L. et al. Imaging defects and their evolution in a metal–organic framework at sub-unit-cell resolution. *Nat. Chem.* **11**, 622–628 (2019).
75. Koo, J. et al. Hollowing out MOFs: hierarchical micro- and mesoporous MOFs with tailorable porosity via selective acid etching. *Chem. Sci.* **8**, 6799–6803 (2017).
76. Gong, X. et al. Metal-organic frameworks for the exploit of distance between active sites in efficient photocatalysis. *Angew. Chem. Int. Ed.* **59**, 5326–5331 (2020).
77. Luo, L. et al. Directional engraving within single crystalline metal–organic framework particles via oxidative linker cleaving. *J. Am. Chem. Soc.* **141**, 20365–20370 (2019).
78. Yan, J., MacDonald, J. C., Maag, A. R., Coudert, F.-X. & Burdette, S. C. MOF decomposition and introduction of repairable defects using a photodegradable strut. *Chem. Eur. J.* **25**, 8393–8400 (2019).
79. Feng, L. et al. Creating hierarchical pores by controlled linker thermolysis in multivariate metal–organic frameworks. *J. Am. Chem. Soc.* **140**, 2363–2372 (2018).
80. Yuan, S. et al. Construction of hierarchically porous metal–organic frameworks through linker labilization. *Nat. Commun.* **8**, 15356 (2017).
81. Guillerm, V., Xu, H., Albalad, J., Imaz, I. & Maspoch, D. Postsynthetic selective ligand cleavage by solid–gas phase ozonolysis fuses micropores into mesopores in metal–organic frameworks. *J. Am. Chem. Soc.* **140**, 15022–15030 (2018).
82. Tu, B. et al. Ordered vacancies and their chemistry in metal–organic frameworks. *J. Am. Chem. Soc.* **136**, 14465–14471 (2014).
83. Yuan, S. et al. Sequential linker installation: precise placement of functional groups in multivariate metal–organic frameworks. *J. Am. Chem. Soc.* **137**, 3177–3180 (2015).
84. Zhang, X., Frey, B. L., Chen, Y.-S. & Zhang, J. Topology-guided stepwise insertion of three secondary linkers in zirconium metal–organic frameworks. *J. Am. Chem. Soc.* **140**, 7710–7715 (2018).
85. Pang, J. et al. Enhancing pore-environment complexity using a trapezoidal linker: toward stepwise assembly of multivariate quinary metal–organic frameworks. *J. Am. Chem. Soc.* **140**, 12328–12332 (2018).
86. Kapustin, E. A., Lee, S., Alshammari, A. S. & Yaghi, O. M. Molecular retrofitting adapts a metal–organic framework to extreme pressure. *ACS Cent. Sci.* **3**, 662–667 (2017).
87. Wei, Y.-S. et al. Coordination templated [2+2+2] cyclotrimerization in a porous coordination framework. *Nat. Commun.* **6**, 8348 (2015).
88. Deng, H. et al. Multiple functional groups of varying ratios in metal–organic frameworks. *Science* **327**, 846–850 (2010).
89. Burrows, A. D., Frost, C. G., Mahon, M. F. & Richardson, C. Post-synthetic modification of tagged metal–organic frameworks. *Angew. Chem. Int. Ed.* **47**, 8482–8486 (2008).
90. Kleist, W., Jutz, F., Maciejewski, M. & Baiker, A. Mixed-linker metal-organic frameworks as catalysts for the synthesis of propylene carbonate from propylene oxide and CO_2. *Eur. J. Inorg. Chem.* **2009**, 3552–3561 (2009).
91. Taylor-Pashow, K. M., Della Rocca, J., Xie, Z., Tran, S. & Lin, W. Postsynthetic modifications of iron-carboxylate nanoscale metal–organic frameworks for imaging and drug delivery. *J. Am. Chem. Soc.* **131**, 14261–14263 (2009).
92. Burrows, A. D. Mixed-component metal–organic frameworks (MC-MOFs): enhancing functionality through solid solution formation and surface modifications. *CrystEngComm.* **13**, 3623–3642 (2011).

93. Zhang, Y.-B. et al. Introduction of functionality, selection of topology, and enhancement of gas adsorption in multivariate metal–organic framework-177. *J. Am. Chem. Soc.* **137**, 2641–2650 (2015).
94. Osborn Popp, T. M. & Yaghi, O. M. Sequence-dependent materials. *Acc. Chem. Res.* **50**, 532–534 (2017).
95. Qin, J.-S., Yuan, S., Wang, Q., Alsalme, A. & Zhou, H.-C. Mixed-linker strategy for the construction of multifunctional metal–organic frameworks. *J. Mater. Chem. A* **5**, 4280–4291 (2017).
96. Kong, X. et al. Mapping of functional groups in metal–organic frameworks. *Science* **341**, 882–885 (2013).
97. Choi, K. M., Na, K., Somorjai, G. A. & Yaghi, O. M. Chemical environment control and enhanced catalytic performance of platinum nanoparticles embedded in nanocrystalline metal–organic frameworks. *J. Am. Chem. Soc.* **137**, 7810–7816 (2015).
98. Kalaj, M., Palomba, J. M., Bentz, K. C. & Cohen, S. M. Multiple functional groups in UiO-66 improve chemical warfare agent simulant degradation. *Chem. Commun.* **55**, 5367–5370 (2019).
99. Dong, D., Sun, Y., Chu, J., Zhang, X. & Deng, H. Multivariate metal–organic frameworks for dialing-in the binding and programming the release of drug molecules. *J. Am. Chem. Soc.* **39**, 14209–14216 (2017).
100. Newsome, W. J. et al. Solid state multicolor emission in substitutional solid solutions of metal-organic frameworks. *J. Am. Chem. Soc.* **141**, 11298–11303 (2019).
101. Li, B. et al. Porous metal–organic frameworks with Lewis basic nitrogen sites for high-capacity methane storage. *Energy Environ. Sci.* **8**, 2504–2511 (2015).
102. Kim, M., Cahill, J. F., Fei, H., Prather, K. A. & Cohen, S. M. Postsynthetic ligand and cation exchange in robust metal–organic frameworks. *J. Am. Chem. Soc.* **134**, 18082–18088 (2012).
103. Szilágyi, P. Á. Interplay of linker functionalization and hydrogen adsorption in the metal–organic framework MIL-101. *J. Phys. Chem. C* **118**, 19572–19579 (2014).
104. Jayachandrababu, K. C., Sholl, D. S. & Nair, S. Structural and mechanistic differences in mixed-linker zeolitic imidazolate framework synthesis by solvent assisted linker exchange and de novo routes. *J. Am. Chem. Soc.* **139**, 5906–5915 (2017).
105. Boissonnault, J. A., Wong-Foy, A. G. & Matzger, A. J. Core–shell structures arise naturally during ligand exchange in metal–organic frameworks. *J. Am. Chem. Soc.* **139**, 14841–14844 (2017).
106. Li, T., Kozlowski, M. T., Doud, E. A., Blakely, M. N. & Rosi, N. L. Stepwise ligand exchange for the preparation of a family of mesoporous MOFs. *J. Am. Chem. Soc.* **135**, 11688–11691 (2013).
107. Fracaroli, A. M. et al. Seven post-synthetic covalent reactions in tandem leading to enzyme-like complexity within metal–organic framework crystals. *J. Am. Chem. Soc.* **138**, 8352–8355 (2016).
108. Caskey, S. R. & Matzger, A. J. Selective metal substitution for the preparation of heterobimetallic microporous coordination polymers. *Inorg. Chem.* **47**, 7942–7944 (2008).
109. Serre, C. et al. Synthesis, characterisation and luminescent properties of a new three-dimensional lanthanide trimesate: $M((C_6H_3)\text{-}(CO_2)_3)$ (M = Y, Ln) or MIL-78. *J. Mater. Chem.* **14**, 1540–1543 (2004).
110. de Lill, D. T., de Bettencourt-Dias, A. & Cahill, C. L. Exploring lanthanide luminescence in metal-organic frameworks: synthesis, structure, and guest-sensitized luminescence of a mixed europium/terbium-adipate framework and a terbium-adipate framework. *Inorg. Chem.* **46**, 3960–3965 (2007).
111. Schubert, D. M., Visi, M. Z. & Knobler, C. B. Acid-catalyzed synthesis of zinc imidazolates and related bimetallic metal-organic framework compounds. *Main Group. Chem.* **7**, 311–322 (2008).
112. White, K. A. et al. Near-infrared luminescent lanthanide MOF barcodes. *J. Am. Chem. Soc.* **131**, 18069–18071 (2009).
113. Soares-Santos, P. C. et al. Photoluminescent 3D lanthanide–organic frameworks with 2,5-pyridinedicarboxylic and 1,4-phenylenediacetic acids. *Cryst. Growth Des.* **8**, 2505–2516 (2008).
114. Jee, B. et al. Continuous wave and pulsed electron spin resonance spectroscopy of paramagnetic framework cupric ions in the Zn(II) doped porous coordination polymer $Cu_{3-x}Zn_x(btc)_2$. *J. Phys. Chem. C* **114**, 16630–16639 (2010).
115. Wang, L. J. et al. Synthesis and characterization of metal–organic framework-74 containing 2, 4, 6, 8, and 10 different metals. *Inorg. Chem.* **53**, 5881–5883 (2014).
116. Liu, Q., Cong, H. & Deng, H. Deciphering the spatial arrangement of metals and correlation to reactivity in multivariate metal–organic frameworks. *J. Am. Chem. Soc.* **138**, 13822–13825 (2016).
117. Castillo-Blas, C. et al. Addressed realization of multication complex arrangements in metal–organic frameworks. *Sci. Adv.* **3**, e1700773 (2017).
118. Jiao, Y. et al. Tuning the kinetic water stability and adsorption interactions of Mg-MOF-74 by partial substitution with Co or Ni. *Ind. Eng. Chem. Res.* **54**, 12408–12414 (2015).
119. Botas, J. A., Calleja, G., Sánchez-Sánchez, M. & Orcajo, M. G. Cobalt doping of the MOF-5 framework and its effect on gas-adsorption properties. *Langmuir* **26**, 5300–5303 (2010).
120. Zhai, Q.-G., Bu, X., Mao, C., Zhao, X. & Feng, P. Systematic and dramatic tuning on gas sorption performance in heterometallic metal–organic frameworks. *J. Am. Chem. Soc.* **138**, 2524–2527 (2016).
121. Xia, Q. et al. Multivariate metal–organic frameworks as multifunctional heterogeneous asymmetric catalysts for sequential reactions. *J. Am. Chem. Soc.* **139**, 8259–8266 (2017).
122. Evans, J. D., Sumby, C. J. & Doonan, C. J. Post-synthetic metalation of metal–organic frameworks. *Chem. Soc. Rev.* **43**, 5933–5951 (2014).
123. Das, S., Kim, H. & Kim, K. Metathesis in single crystal: complete and reversible exchange of metal ions constituting the frameworks of metal–organic frameworks. *J. Am. Chem. Soc.* **131**, 3814–3815 (2009).
124. Brozek, C. K. & Dincă, M. Ti^{3+}-, $V^{2+/3+}$-, $Cr^{2+/3+}$-, Mn^{2+}-, and Fe^{2+}-substituted MOF-5 and redox reactivity in Cr- and Fe-MOF-5. *J. Am. Chem. Soc.* **135**, 12886–12891 (2013).
125. Liu, T.-F. et al. Stepwise synthesis of robust metal–organic frameworks via postsynthetic metathesis and oxidation of metal nodes in a single-crystal to single-crystal transformation. *J. Am. Chem. Soc.* **136**, 7813–7816 (2014).
126. Bloch, E. D. et al. Metal insertion in a microporous metal–organic framework lined with 2,2′-bipyridine. *J. Am. Chem. Soc.* **132**, 14382–14384 (2010).
127. Tan, C., Han, X., Li, Z., Liu, Y. & Cui, Y. Controlled exchange of achiral linkers with chiral linkers in Zr-based UiO-68 metal–organic framework. *J. Am. Chem. Soc.* **140**, 16229–16236 (2018).
128. Nguyen, H. G. T. et al. Vanadium-node-functionalized UiO-66: a thermally stable MOF-supported catalyst for the gas-phase oxidative dehydrogenation of cyclohexene. *ACS Catal.* **4**, 2496–2500 (2014).
129. Kim, I. S. et al. Targeted single-site MOF node modification: trivalent metal loading via atomic layer deposition. *Chem. Mater.* **27**, 4772–4778 (2015).
130. Manna, K. et al. Chemoselective single-site Earth-abundant metal catalysts at metal–organic framework nodes. *Nat. Commun.* **7**, 12610 (2016).
131. Ji, P. et al. Single-site cobalt catalysts at new $Zr_{12}(\mu_3\text{-}O)_8(\mu_3\text{-}OH)_8(\mu_2\text{-}OH)_6$ metal–organic framework nodes for highly active hydrogenation of nitroarenes, nitriles, and isocyanides. *J. Am. Chem. Soc.* **139**, 7004–7011 (2017).
132. Manna, K., Ji, P., Greene, F. X. & Lin, W. Metal–organic framework nodes support single-site magnesium–alkyl catalysts for hydroboration and hydroamination reactions. *J. Am. Chem. Soc.* **138**, 7488–7491 (2016).
133. Krajnc, A., Kos, T., Zabukovec Logar, N. & Mali, G. A simple NMR based method for studying the spatial distribution of linkers within mixed-linker metal–organic frameworks. *Angew. Chem. Int. Ed.* **54**, 10535–10538 (2015).
134. Jayachandrababu, K. C. et al. Structure elucidation of mixed-linker zeolitic imidazolate frameworks by solid-state ^{1}H CRAMPS NMR spectroscopy and computational modeling. *J. Am. Chem. Soc.* **138**, 7325–7336 (2016).
135. Schrimpf, W. et al. Chemical diversity in a metal–organic framework revealed by fluorescence lifetime imaging. *Nat. Commun.* **9**, 1647 (2018).
136. Zhao, Y. et al. Mesoscopic constructs of ordered and oriented metal–organic frameworks on plasmonic silver nanocrystals. *J. Am. Chem. Soc.* **137**, 2199–2202 (2015).
137. Schneemann, A. et al. Flexible metal–organic frameworks. *Chem. Soc. Rev.* **43**, 6062–6096 (2014).
138. Horike, S., Shimomura, S. & Kitagawa, S. Soft porous crystals. *Nat. Chem.* **1**, 695–704 (2009).
139. Deng, H., Olson, M. A., Stoddart, J. F. & Yaghi, O. M. Robust dynamics. *Nat. Chem.* **2**, 439–443 (2010).
140. Serre, C. et al. Very large breathing effect in the first nanoporous chromium(III)-based solids: MIL-53 or $Cr^{III}(OH)\cdot\{O_2C\text{–}C_6H_4\text{–}CO_2\}\cdot\{HO_2C\text{–}C_6H_4\text{–}CO_2H\}_x\cdot H_2O_y$. *J. Am. Chem. Soc.* **124**, 13519–13526 (2002).
141. Maji, T. K., Matsuda, R. & Kitagawa, S. A flexible interpenetrating coordination framework with a bimodal porous functionality. *Nat. Mater.* **6**, 142–147 (2007).
142. Liu, Y. et al. Weaving of organic threads into a crystalline covalent organic framework. *Science* **351**, 365–369 (2016).
143. Coskun, A. et al. Metal–organic frameworks incorporating copper-complexed rotaxanes. *Angew. Chem. Int. Ed.* **51**, 2160–2163 (2012).
144. Park, J. et al. Reversible alteration of CO_2 adsorption upon photochemical or thermal treatment in a metal–organic framework. *J. Am. Chem. Soc.* **134**, 99–102 (2012).
145. Whitesides, G. M. & Grzybowski, B. Self-assembly at all scales. *Science* **295**, 2418–2421 (2002).
146. Park, J., Feng, D., Yuan, S. & Zhou, H.-C. Photochromic metal–organic frameworks: reversible control of singlet oxygen generation. *Angew. Chem. Int. Ed.* **54**, 430–435 (2015).
147. Williams, D. E. et al. Energy transfer on demand: photoswitch-directed behavior of metal–porphyrin frameworks. *J. Am. Chem. Soc.* **136**, 11886–11889 (2014).
148. Walton, I. M. et al. The role of atropisomers on the photo-reactivity and fatigue of diarylethene-based metal–organic frameworks. *New J. Chem.* **40**, 101–106 (2014).
149. Brown, J. W. et al. Photophysical pore control in an azobenzene-containing metal–organic framework. *Chem. Sci.* **4**, 2858–2864 (2013).
150. Danowski, W. et al. Unidirectional rotary motion in a metal–organic framework. *Nat. Nanotechnol.* **14**, 488–494 (2019).
151. Zhu, K., O'Keefe, C. A., Vukotic, V. N., Schurko, R. W. & Loeb, S. J. A molecular shuttle that operates inside a metal–organic framework. *Nat. Chem.* **7**, 514–519 (2015).
152. Chen, Q. et al. A redox-active bistable molecular switch mounted inside a metal–organic framework. *J. Am. Chem. Soc.* **138**, 14242–14245 (2016).

Acknowledgements
The authors acknowledge King Abdulaziz City for Science and Technology (KACST) as part of a joint KACST–UC Berkeley collaboration, the National Natural Science Foundation of China (21522105, 21922103, 21961132003, 21971199 and 91622103), the National Key R&D Program of China (2018YFA0704000) and the Science & Technology Commission of Shanghai Municipality (17JC1400100 and 17JC1404000).

Author contributions
All authors researched data for the article and contributed to the discussion of content, and writing and editing of the manuscript.

Competing interests
The authors declare no competing interests.

Publisher's note
Springer Nature remains neutral with regard to jurisdictional claims in published maps and institutional affiliations.